An adaptive Newton continuation strategy for the fully implicit finite element immersed boundary method

R.H.W. Hoppe [a,b,*], C. Linsenmann [b]

[a] Department of Mathematics, University of Houston, PGH 651, Houston, TX 77204-3008, USA
[b] Institute of Mathematics, University of Augsburg, Universitätsstr. 14, D-86159 Augsburg, Germany

1. Introduction

A computationally attractive methodology for the numerical simulation of the motion and deformation of elastic and viscoelastic bodies in external flows is the immersed boundary method (IB), which has been originally developed by Peskin [31] and further studied in [11,32–34,36]. The IBM uses an Eulerian coordinate system for the flow equations and Lagrangian coordinates for the boundary of the immersed bodies together with appropriate interaction equations to transform Eulerian to Lagrangian quantities and vice versa. The interaction equations feature multidimensional Dirac delta functions that have to be approximated appropriately within a finite difference approach. More recently, a variational formulation of the IBM has been provided in [8–10] as a basis for a finite element realization referred to as the Finite Element Immersed Boundary Method (FE-IB). Both for the classical IB and the FE-IB, the most common approach with regard to discretization in time is to use the Backward Euler (BE) method for the flow equations and the Forward Euler (FE) method for the equation describing the motion and deformation of the immersed bodies which gives rise to the BE/FE IB and BE/FE FE-IB, respectively. However,

* Corresponding author at: Department of Mathematics, University of Houston, PGH 651, Houston, TX 77204-3008, USA. Tel.: +49 821 598 2194/+1 713 743 3452; fax: +49 821 598 2193/+1 713 743 3505.
E-mail addresses: rohop@math.uh.edu, hoppe@math.uni-augsburg.de (R.H.W. Hoppe), linsenmann@math.uni-augsburg.de (C. Linsenmann).

these schemes typically require a CFL-type condition (cf., e.g., [9,16]). Better stability properties can be achieved by using the BE method as a time integrator for both equations thus resulting in a fully implicit scheme. Recent applications of the BE/BE IB can be found in [25–28], whereas the unconditional stability of the BE/BE FE-IB has been shown in [9]. For each time step, the implementation of the fully implicit scheme requires the solution of a nonlinear system of equations for which a Newton-type method would be the method of choice using the result of the previous step as an initial guess. Sudden changes in the energy of the system, for instance due to large deformations of the immersed bodies, may lead to significant restrictions of the time step size in order to guarantee convergence of the Newton-type iteration. Such scenarios can be handled adequately by an adaptive choice of the time step size which can be realized by treating the problem as a parameter dependent one and using a predictor–corrector continuation in time based on the affine covariant convergence theory of Newton-type methods (cf., e.g., [15] and the references therein). It is the purpose of this contribution to provide such an adaptive continuation strategy for the fully implicit FE-IB. The paper is organized as follows:

In Section 2, we begin with a brief overview on the FE-IB which is based on the variational formulation of the problem (Section 2.1) and then derive the fully implicit scheme giving rise to the solution of a nonlinear system of equations at each time step (Section 2.2). In particular, we show that the associated nonlinear map admits an invertible Jacobian under some constraints on the time step size (Theorem 2.5) and discuss scenarios for which we may encounter severe time step restrictions. Section 3 is devoted to the adaptive continuation method which is a predictor–corrector continuation method in time. It uses classical continuation as a predictor and a combination of the ordinary and the simplified Newton method as a corrector featuring an adaptive choice of the continuation steplength based on information of the previous successful continuation step and a monotonicity test for convergence monitoring. In Section 4, we provide two representative examples, namely the motion and deformation of a red blood cell through a thin capillary (Example 1) and under the influence of a quadrupolar fluid force (Example 2). We address the shortcomings of the BE/FE FE-IB and illustrate the superior performance of the adaptive continuation approach based on the fully implicit scheme.

2. Finite element immersed boundary method

We consider the motion and deformation of viscoelastic bodies such as vesicles and red blood cells immersed in an incompressible external fluid. The classical IB as developed in [31] uses three groups of equations:

- the incompressible Navier–Stokes equations describing the motion of the fluid within an Eulerian coordinate system,
- the material elasticity equations describing the deformation of the immersed bodies in terms of the change of the total elastic energy within a Lagrangian coordinate system,
- the interaction equations which transform Eulerian into Lagrangian quantities and vice versa.

The FE-IB has been originally studied in [8] and [9]. It relies on the variational formulation of these equations which will be addressed in Section 2.1. The fully implicit FE-IB which will be dealt with in Section 2.2 is based on finite element approximations of the variational equations in space and implicit time discretizations by the Backward Euler (BE) scheme both for the semi-discretized Navier–Stokes and interaction equations. Therefore, it will be referred to as the BE/BE FE-IB.

2.1. Variational formulation of the IB

We assume $\Omega = (a,b) \times (c,d)$, $a < b$, $c < d$, to be a domain in $\mathbb{R}^2$ with boundary $\Gamma = \overline{\Gamma}_{\text{in}} \cup \overline{\Gamma}_{\text{lat}} \cup \overline{\Gamma}_{\text{out}}$, where $\Gamma_{\text{in}} := \{a\} \times (c,d)$, $\Gamma_{\text{out}} := \{b\} \times (c,d)$, and $\Gamma_{\text{lat}} := \Gamma_{\text{bot}} \cup \Gamma_{\text{top}}$, $\Gamma_{\text{bot}} := (a,b) \times \{c\}$,$\Gamma_{\text{top}} := (a,b) \times \{d\}$. We set $Q := \Omega \times (0,T)$,$\Sigma_{\text{in}} := \Gamma_{\text{in}} \times (0,T)$,$\Sigma_{\text{lat}} := \Gamma_{\text{lat}} \times (0,T)$,$\Sigma_{\text{out}} := \Gamma_{\text{out}} \times (0,T)$, where $T > 0$. We assume that the fluids has density $\rho > 0$ and dynamic viscosity $\eta > 0$. We denote by $\mathbf{u} = \mathbf{u}(x,t)$ and $p = p(x,t)$, $(x,t) \in Q$, the velocity and the pressure. We further refer to $\boldsymbol{\varepsilon}(\mathbf{u}) := (\nabla \mathbf{u} + (\nabla \mathbf{u})^T)/2$ as the linearized strain tensor and to $\boldsymbol{\sigma}(\mathbf{u},p) := -p\mathbf{I} + 2\nu\boldsymbol{\varepsilon}(\mathbf{u})$ as the stress tensor. Assuming a force density $\mathbf{F}$ in Q, periodic boundary conditions in terms of a prescribed stationary velocity $\mathbf{g}$ at the inflow boundary Σ_{in} and the outflow boundary Σ_{out}, zero velocity on Σ_{lat}, and an initial velocity $\mathbf{u}^{(0)}$ at time $t = 0$, the incompressible Navier Stokes equations read

$$\rho\left(\frac{\partial \mathbf{u}}{\partial t} + (\mathbf{u} \cdot \nabla)\mathbf{u}\right) - \eta\Delta\mathbf{u} + \nabla p = \mathbf{F} \quad \text{in} \quad Q, \tag{2.1a}$$

$$\nabla \cdot \mathbf{u} = 0 \quad \text{in} \quad Q, \tag{2.1b}$$

$$\mathbf{u} = \mathbf{g} = (g,0)^T, \quad g \geqslant 0 \quad \text{on} \quad \Sigma', \ \Sigma' \in \{\Sigma_{\text{in}}, \Sigma_{\text{out}}\}, \tag{2.1c}$$

$$\mathbf{u} = \mathbf{0} \quad \text{on} \quad \Sigma_{\text{lat}}, \tag{2.1d}$$

$$\mathbf{u}(\cdot,0) = \mathbf{u}^{(0)} \quad \text{in} \quad \Omega. \tag{2.1e}$$

For the variational formulation of (2.1a)–(2.1e) we use standard notation from Lebesgue and Sobolev space theory (cf., e.g., [18,40]). In particular, for a bounded domain $\Omega \subset \mathbb{R}^d$, $d \in \mathbb{N}$, we denote by $L^p(\Omega)$ and $\mathbf{L}^p(\Omega) := L^p(\Omega)^d$,$1 \leqslant p \leqslant \infty$, the Banach space of to the power p square integrable scalar- and vector-valued functions on Ω. In particular, for $p = 2$ the spaces $L^2(\Omega)$ and $\mathbf{L}^2(\Omega)$ are Hilbert spaces, equipped with the inner product $(\cdot,\cdot)_{0,\Omega}$ and the associated norm $\|\cdot\|_{0,\Omega}$. $L^2_0(\Omega)$ stands for the

subspace of functions with zero integral mean. Further, we denote by $\mathbf{H}^s(\Omega),\ s\in\mathbb{R}_+$, the Sobolev space of vector-valued functions with the inner product $(\cdot,\cdot)_{s,\Omega}$and the associated norm $\|\cdot\|_{s,\Omega}$. The space $\mathbf{H}^s_{0,\Gamma'}(\Omega)$ is the subspace with vanishing trace on $\Gamma'\subseteq\ \Gamma$. We will omit the subindex Γ', if $\Gamma'=\Gamma$. $\mathbf{H}^{-s}(\Omega)$ stands for the dual space of $\mathbf{H}^s_0(\Omega)$ with $\langle\cdot,\cdot\rangle$ referring to the dual product. The space $\mathbf{H}^s(\overline{\Omega})\subset\mathbf{H}^s(\Omega)$ is the subspace of all $\mathbf{u}|_\Omega$ where $\mathbf{u}\in\mathbf{H}^s(\mathbb{R}^d)$ and $\langle\mathbf{u}|_\Omega,\boldsymbol{\varphi}\rangle=\langle\mathbf{u},\tilde{\boldsymbol{\varphi}}\rangle$ for all $\boldsymbol{\varphi}\in\mathbf{C}^\infty_0(\Omega)$ with $\tilde{\boldsymbol{\varphi}}$ referring to the continuation of $\boldsymbol{\varphi}$ by zero outside Ω. We denote by$\mathbf{H}^{s-1/2}(\Gamma'),s\geqslant 1$, the trace space of vector-valued functions on Γ'. We further refer to $\mathbf{H}^{s-1/2}_{00}(\Gamma')$ as the space of functions whose extensions by zero to $\Gamma\backslash\Gamma'$ belong to $\mathbf{H}^{s-1/2}(\Gamma)$. Finally, we denote by $C^k(\Omega)$ and $\mathbf{C}^k(\Omega),\ k\in\mathbb{N}_0$ the Banach spaces of k-times continuously differentiable scalar- and vector-valued functions on Ω.

Moreover, for $T>0$ and a Banach space $Z(\mathbf{Z})$ of scalar (vector-valued) functions, we denote by $L^2((0,T),Z)$ ($\mathbf{L}^2((0,T),\mathbf{Z})$ the Hilbert space and by $C([0,T];Z)(\mathbf{C}([0,T],\mathbf{Z}))$ the Banach space of functions $v\colon\ [0,T]\to Z(\mathbf{v}:[0,T]\to\mathbf{Z})$. The spaces $H^s((0,T),Z),\ s\in\mathbb{R}_+,\ (\mathbf{H}^s((0,T),\mathbf{Z}))$ are defined likewise.

We introduce the function spaces

$$\begin{aligned}\mathbf{V}(0,T)\ &:=\ \mathbf{H}^1((0,T),\mathbf{H}^{-1}(\Omega))\cap\mathbf{L}^2((0,T),\mathbf{H}^1(\Omega)),\\ \mathbf{W}(0,T)\ &:=\ \{\mathbf{w}\in\mathbf{V}(0,T)|\mathbf{w}|_{\Sigma'}=\mathbf{g},\mathbf{w}|_{\Sigma_{\text{lat}}}=\mathbf{0}\},\\ Q(0,T)\ &:=\ L^2((0,T),L^2_0(\Omega)),\end{aligned}$$

where $\Sigma'=\Sigma_{\text{in}}\cup\Sigma_{\text{out}}$. Assuming $\mathbf{F}(t)\in\mathbf{H}^{-1}(\Omega)),\ \mathbf{g}(t)\in\mathbf{H}^{1/2}_{00}(\Sigma'),\ t\in(0,T)$, and $\mathbf{u}^{(0)}\in\mathbf{L}^2(\Omega)$, the weak formulation of the Navier–Stokes equations (2.1a)–(2.1e) requires the computation of $(\mathbf{u},p)\in(\mathbf{W}(0,T)\cap\mathbf{L}^\infty(Q))\times Q(0,T)$ such that for all $\mathbf{v}\in\mathbf{H}^1_0(\Omega)$ and $w\in L^2_0(\Omega)$ there holds

$$\left\langle\rho\frac{\partial\mathbf{u}}{\partial t},\mathbf{v}\right\rangle+a(\mathbf{u},\mathbf{v})-b(p,\mathbf{v})=\ell(\mathbf{v}),\tag{2.2a}$$

$$b(w,\mathbf{u})=0,\tag{2.2b}$$

$$\mathbf{u}(\cdot,0)=\mathbf{u}^{(0)}.\tag{2.2c}$$

Here, $a(\cdot,\cdot)$, $b(\cdot,\cdot)$, and the functional $\ell(\cdot)$ are given by

$$a(\mathbf{u},\mathbf{v})\ :=\ (\rho(\mathbf{u}\cdot\nabla)\mathbf{u},\mathbf{v})_{0,\Omega}+(\eta\nabla\mathbf{u},\nabla\mathbf{v})_{0,\Omega}\tag{2.3a}$$

$$b(p,\mathbf{v})\ :=\ (p,\nabla\cdot\mathbf{v})_{0,\Omega},\quad \ell(v)\ :=\ \langle\mathbf{F},\mathbf{v}\rangle.\tag{2.3b}$$

We further suppose that Ω is filled with a suspension of N viscoelastic particles immersed in the carrier fluid such that the subdomains $B^{(i)}_t\subset\Omega, 1\leqslant i\leqslant N$, with $\overline{B}^{(i)}_t\cap\overline{B}^{(j)}_t=\emptyset, 1\leqslant i\neq j\leqslant N$, describe the spatial location of the particles at time $t\in[0,T]$. The boundaries $\partial B^{(i)}_t$ are supposed to be non-selfintersecting closed curves. For ease of notation, we consider the case $N=1$ and write B_t instead of $B^{(1)}_t$. The generalization to $N>1$ is obvious. We assume that the boundary ∂B_0 of the initial configuration B_0 has length $L:=|\partial B_0|$ and denote by $q\in[0,L]$ the Lagrangian coordinate labeling a material point on ∂B_0. We further refer to $\mathbf{X}(q,,t)=(X_1(q,t),X_2(q,t))^T$ as the position of that point at time $t\in(0,T]$. We denote by

$$\mathcal{E}^e(\mathbf{X}(q,t))=\frac{\kappa_e}{2}\left|\frac{\partial\mathbf{X}}{\partial q}(q,t)\right|^2,\quad \mathcal{E}^b(\mathbf{X}(q,t))=\frac{\kappa_b}{2}\left|\frac{\partial^2\mathbf{X}}{\partial q^2}(q,t)\right|^2,\tag{2.4}$$

the local energy densities on the immersed elastic boundary $\partial\, B_t$, where $\kappa_e>0$ and $\kappa_b>0$ denotes the elasticity coefficient with respect to elongation-compression and bending, respectively. Then,

$$E(t)\ :=\ E_e(t)+E_b(t),\ t\in(0,T),\tag{2.5}$$

$$E^e(t)\ :=\ \int_0^L\mathcal{E}^e(\mathbf{X}(q,t))dq,\quad E^b(t)\ :=\ \int_0^L\mathcal{E}^b(\mathbf{X}(q,t))dq,$$

is the associated total energy consisting of the elastic energy $E^e(t)$ and the bending energy $E^b(t)$. The local force density $\mathbf{f}$ is given by $\mathbf{f}(q,t)=-E'(\mathbf{X}(q,t))$, where E' stands for the the Gâteaux derivative of E.

We introduce the function space

$$\mathbf{H}^2_{\text{per}}([0,L])\ :=\ \{\mathbf{Y}\in\mathbf{H}^2((0,L))|\partial^k\mathbf{Y}(0)/\partial q^k=\partial^k\mathbf{Y}(L)/\partial q^k,\ k=0,1\},\tag{2.6}$$

and we require

$$\mathbf{X}\in\mathbf{H}^1((0,T),\mathbf{L}^2([0,L]))\cap\mathbf{L}^2\Big((0,T),\mathbf{H}^2_{\text{per}}([0,L])\Big).\tag{2.7}$$

In view of (2.4) and (2.5) and $\mathbf{f}(\cdot,t)=-E'\ (\mathbf{X}(\cdot,t))$ we have $\mathbf{f}(\cdot,t)\in\mathbf{H}_{\text{per}}{}^2\ ([0,L])^*$. Then, assuming some initial configuration $\mathbf{X}^{(0)}\in\mathbf{H}_{\text{per}}{}^2([0,L])$, the variational formulation of the interaction equations reads

$$\langle\mathbf{F}(t),\mathbf{v}\rangle=\langle\mathbf{f}(\cdot,t),\mathbf{v}(\mathbf{X}(\cdot,t))\rangle,\tag{2.8a}$$

for all $\mathbf{v}\in\mathbf{H}^{2+\mu}(\Omega)\cap\mathbf{H}^1_0(\Omega),\ \mu\geqslant 1/2$, such that $\mathbf{v}|_{\partial B_t}\in\mathbf{H}^2_{\text{per}}([0,L])$, and

$$\int_0^L \frac{\partial \mathbf{X}}{\partial t}(q,t)\cdot\mathbf{Y}(q)dq = \int_0^L \mathbf{u}(\mathbf{X}(q,t),t)\cdot\mathbf{Y}(q)dq, \tag{2.8b}$$

$$\int_0^L \mathbf{X}(q,0)\cdot\mathbf{Y}(q)dq = \int_0^L \mathbf{X}^{(0)}(q)\cdot\mathbf{Y}(q)dq \tag{2.8c}$$

for all $\mathbf{Y}\in {\mathbf{H}_{\text{per}}}^2([0,L])$.

Remark 2.1. We note that in contrast to the FE-IB approach in [8], here and in the sequel we use the variational rather than the pointwise formulation of the motion of the immersed body (cf. (2.8b) and (2.8c)).

Remark 2.2. If we use (2.4) in (2.8a), for sufficiently smooth $\mathbf{v}$ we obtain

$$\begin{aligned}\langle \mathbf{F}(t),\mathbf{v}\rangle = & -\kappa_e\int_0^L \frac{\partial \mathbf{X}(\cdot,t)}{\partial q}\cdot \mathbf{D}^1\mathbf{v}(\mathbf{X}(\cdot,t))\frac{\partial \mathbf{X}(\cdot,t)}{\partial q}dq\\ & -\kappa_b\int_0^L \frac{\partial^2 \mathbf{X}(\cdot,t)}{\partial q^2}\cdot \mathbf{D}^1\mathbf{v}(\mathbf{X}(\cdot,t))\frac{\partial^2 \mathbf{X}(\cdot,t)}{\partial q^2}dq\\ & -\kappa_b\int_0^L \frac{\partial^2 \mathbf{X}(\cdot,t)}{\partial q^2}\cdot \mathbf{D}^2\mathbf{v}(\mathbf{X}(\cdot,t))\left(\frac{\partial \mathbf{X}(\cdot,t)}{\partial q},\frac{\partial \mathbf{X}(\cdot,t)}{\partial q}\right)dq.\end{aligned} \tag{2.9}$$

2.2. Fully implicit FE-IB

We assume $\mathcal{T}_h(\Omega)$ to be a simplicial triangulation of Ω that aligns with the partition of Γ. For $D\subseteq\overline{\Omega}$, we refer to $\mathcal{T}_h(D)$ as the union of triangles that have nonzero intersection with D, i.e.,

$$\mathcal{T}_h(D) = \bigcup\{T\in\mathcal{T}_h(\Omega)|T\cap D\neq\emptyset\}. \tag{2.10}$$

For $T\in\mathcal{T}_h(\Omega)$, we denote by $|T|$ the area of T and by h_T the diameter of T. We set $h := \max\{h_T|T\in\mathcal{T}_h(\Omega)\}$. Further, $P_k(T),\ k\in\mathbb{N}$, refers to the set of polynomials of degree $\leqslant k$ on T. We suppose that $\mathcal{T}_h(\Omega)$is quasi-uniform, i.e., there exist constants $0<c_Q\leqslant C_Q$ that only depend on the local geometry of the triangulation such that

$$c_Q h\leqslant h_T\leqslant C_Q h,\ T\in\mathcal{T}_h(\Omega). \tag{2.11}$$

For the spatial discretization of the weak formulation (2.2a), (2.2b) of the incompressible Navier–Stokes equations we use P2-P1 Taylor–Hood elements [14], i.e., we define

$$\begin{aligned}V_h &:= \{v_h\in C(\overline{\Omega})|{v_h}|_T\in P_2(T),\ T\in\mathcal{T}_h(\Omega)\},\\ \mathbf{V}_h &:= \{\mathbf{v}_h\in\mathbf{C}(\overline{\Omega})|\mathbf{v}_h=(v_{h,1},v_{h,2})^T,\ v_{h,v}\in V_h\},\\ Q_h &:= \{w_h\in C(\overline{\Omega})|{w_h}|_T\in P_1(T),\quad T\in\mathcal{T}_h(\Omega)\}\cap L_0^2(\Omega),\end{aligned}$$

and set $\mathbf{V}_{h,0} := \mathbf{V}_h\cap\mathbf{C}_0(\overline{\Omega})$. The finite element spaces V_h and Q_h are spanned by the canonically specified nodal basis functions $\varphi_h^{(i)}, 1\leqslant i\leqslant n_1$, and $\psi_h^{(i)}, 1\leqslant i\leqslant N_2$.

Assuming $\mathbf{g}_h$ to be the quadratic spline interpoland of $\mathbf{g}$ with respect to $\mathcal{T}_h(\Omega)|_{\Gamma'}$, $\Gamma'=\Gamma_{\text{in}}$ resp. $\Gamma'=\Gamma_{\text{out}}$, we set

$$\mathbf{W}_h(0,T) := \{\mathbf{w}_h\in\mathbf{C}([0,T],\mathbf{C}(\overline{\Omega}))|\mathbf{w}_h(\cdot,t)|_T\in\mathbf{V}_h,\mathbf{w}_h(\cdot,t)|_{\Gamma'}=\mathbf{g}_h(\cdot),t\in[0,T],\mathbf{w}_h|_{\Sigma_{\text{lat}}}=\mathbf{0}\},$$

$$Q_h(0,T) := \{w_h\in C([0,T];C(\overline{\Omega}))|w_h(\cdot,t)|_T\in Q_h,t\in[0,T]\}.$$

The discretization of the immersed boundary is done with respect to a partition

$$\mathcal{T}_{\Delta q} := \{0=:q_0<q_1<\cdots<q_{n_3} := L\},\ n_3\in\mathbb{N},$$

of the interval $[0,L]$ into subintervals $I_i := [q_{i-1},q_i], 1\leqslant i\leqslant n_3$, of length $\Delta q_i := q_i-q_{i-1}$ with $\Delta q := \max\{\Delta q_i|1\leqslant i\leqslant n_3\}$. We approximate $\mathbf{X}$from (2.7) by periodic cubic splines and thus define

$$\mathbf{S}_h := \{\mathbf{Y}_h\in\mathbf{C}^2([0,L];\Omega)|\mathbf{Y}_h|_{I_i}\in P_3(I_i)^2, 1\leqslant i\leqslant m_3, \mathbf{Y}_h^{(k)}(q_0)=\mathbf{Y}_h^{(k)}(q_M), k=0,1,2\},$$

where $P_3(I_i)$ stands for the set of polynomials of degree $\leqslant 3$ on I_i. By $\chi_h^{(i)},\ 1\leqslant i\leqslant n_3$, we denote the canonical basis functions (B-splines) spanning the scalar-valued counterpart of $\mathbf{S}_h$. The discrete immersed body occupies subdomains $B_{h,t}\subset\Omega,\ t\in[0,T]$, with boundaries $\partial B_{h,t}$that are C^2 curves described by the periodic cubic spline $\mathbf{X}_h(\cdot,t)\in\mathbf{S}_h$.

We further consider a partitioning $\{0=:t_0<t_1<\cdots<t_M:=T\}$ of the time interval $[0,T]$ with step sizes $\tau_k := t_{k+1}-t_k, 0\leqslant k\leqslant M-1$, and approximate the time derivatives $\partial\mathbf{u}_h/\partial t$ and $\partial\mathbf{X}_h/\partial t$ at $t_{k+1}$by the backward difference quotient. Denoting by $\mathbf{u}_h^{(k)}\in\mathbf{V}_h, p_h^{(k)}\in Q_h$,

and $\mathbf{X}_h^{(k)} \in \mathbf{S}_h$, $0 \leqslant k \leqslant M$, approximations of $\mathbf{u}(\cdot,t_k)$, $p(\cdot,t_k)$, and $\mathbf{X}(\cdot,t_k)$, the fully implicit FE-IB method (BE/BE FE-IB) amounts to the computation of $\left(\mathbf{u}_h^{(k+1)}, p_h^{(k+1)}, \mathbf{X}_h^{(k+1)}\right)$, $0 \leqslant k \leqslant M-1$, such that for all $\mathbf{v}_h \in \mathbf{V}_{h,0}$,$w_h \in Q_h$, and all $\mathbf{Y}_h \in \mathbf{S}_h$ there holds

$$\rho\left(\mathbf{u}_h^{(k+1)}, \mathbf{v}_h\right)_{0,\Omega} + \tau_k a(\mathbf{u}_h^{(k+1)}, \mathbf{v}_h) - \tau_k\ b\left(p_h^{(k+1)}, \mathbf{v}_h\right) = \ell_h(\mathbf{v}_h), \tag{2.12a}$$

$$b\left(w_h, \mathbf{u}_h^{(k+1)}\right) = 0, \tag{2.12b}$$

$$\int_0^L \mathbf{X}_h^{(k+1)} \cdot \mathbf{Y}_h(q)dq - \tau_k \int_0^L \mathbf{u}_h\left(\mathbf{X}_h^{(k+1)}\right) \cdot \mathbf{Y}_h dq = \int_0^L \mathbf{X}_h^{(k)} \cdot \mathbf{Y}_h dq, \tag{2.12c}$$

where the right-hand side in (2.12a) is given by

$$\ell_h(\mathbf{v}_h) := \rho\ (\mathbf{u}_h^{(k)}, \mathbf{v}_h)_{0,\Omega} + \tau_k \int_0^L \mathbf{f}_h^{(k+1)}(q) \cdot \mathbf{v}_h(\mathbf{X}_h^{(k+1)})dq, \tag{2.13}$$

$$\int_0^L \mathbf{f}_h^{(k+1)}(q) \cdot \mathbf{v}_h(\mathbf{X}_h^{(k+1)})dq := -\kappa_e \int_0^L \frac{\partial \mathbf{X}_h^{(k+1)}}{\partial q} \cdot \mathbf{D}^1\mathbf{v}_h(\mathbf{X}_h^{(k+1)}) \frac{\partial \mathbf{X}_h^{(k+1)}}{\partial q} dq,$$

$$- \kappa_b \int_0^L \frac{\partial^2 \mathbf{X}_h^{(k+1)}}{\partial q^2} \cdot \mathbf{D}^1\mathbf{v}_h(\mathbf{X}_h^{(k+1)}) \frac{\partial^2 \mathbf{X}_h^{(k+1)}}{\partial q^2} dq,$$

$$- \kappa_b \int_0^L \frac{\partial^2 \mathbf{X}_h^{(k+1)}}{\partial q^2} \cdot \mathbf{D}^2\mathbf{v}_h\left(\mathbf{X}_h^{(k+1)}\right) \left(\frac{\partial \mathbf{X}_h^{(k+1)}}{\partial q}, \frac{\partial \mathbf{X}_h^{(k+1)}}{\partial q}\right) dq.$$

Remark 2.3. We note that $\mathbf{v}_h \in \mathbf{V}_{h,0}$ does not satisfy $\mathbf{v}_h|_{\partial B_{h,t_{k+1}}} \in \mathbf{H}^2_{\mathrm{per}}([0,L])$ (cf. (2.8a)). However, assuming $\mathrm{meas}m(B_{h,t_{k+1}} \cap \mathcal{E}_h(\Omega)) = \emptyset$, it follows that (2.13) is well defined for $\mathbf{v}_h \in \mathbf{V}_{h,0}$ and $\mathbf{X}_h^{(k+1)} \in \mathbf{S}_h$.

For the algebraic formulation of the BE/BE FE-IB (2.12a)–(2.12c), we introduce the vectors

$$\mathbf{u}^{(k)} := \left(u_1^{(k)}, \cdots, u_{n_1}^{(k)}, u_{n_1+1}^{(k)}, \cdots, u_{N_1}^{(k)}\right)^T,\ 0 \leqslant k \leqslant M,$$

$$\mathbf{p}^{(k)} := \left(p_1^{(k)}, \cdots, p_{N_2}^{(k)}\right)^T,\ 0 \leqslant k \leqslant M,$$

$$\mathbf{X}^{(k)} := \left(X_1^{(k)}, \cdots, X_{n_3}^{(k)}, X_{n_3+1}^{(k)}, \cdots, X_{N_3}^{(k)}\right)^T,\ 0 \leqslant k \leqslant M,$$

the mass matrices $\mathbf{M}_v \in \mathbb{R}^{N_v \times N_v}$, $\mathbf{M}_v = \mathbf{blockdiag}\left(\mathbf{M}_v^{(1)}, \mathbf{M}_v^{(2)}\right), v \in \{1,3\}$, the stiffness matrix $\mathbf{A} \in \mathbb{R}^{N_1 \times N_1}$, $\mathbf{A} = \mathbf{blockdiag}\ (\mathbf{A}^{(1)}, \mathbf{A}^{(2)})$, as well as the matrix $\mathbf{B} \in \mathbb{R}^{N_2 \times N_1}$ by means of

$$\left(\mathbf{M}_1^{(\mu)}\right)_{ij} := \rho \int_\Omega \varphi_h^{(i)} \varphi_h^{(j)}\ d\mathbf{x},\ 1 \leqslant i,j \leqslant n_1,\ 1 \leqslant \mu \leqslant 2,$$

$$\left(\mathbf{M}_3^{(\mu)}\right)_{ij} := \rho \int_0^L \chi_h^{(i)} \chi_h^{(j)} dq,\ 1 \leqslant i,j \leqslant n_3,\ 1 \leqslant \mu \leqslant 2,$$

$$\mathbf{A}_{ij}^{(v)} := v \int_\Omega \nabla\varphi_h^{(i)} \cdot \nabla\varphi_h^{(j)}\ d\mathbf{x},\ 1 \leqslant i,j \leqslant n_1,\ 1 \leqslant v \leqslant 2,$$

$$\mathbf{B}_{ij} := \int_\Omega \frac{\partial \varphi_h^{(j)}}{\partial x_1}\ \psi_h^{(i)}\ d\mathbf{x},\ \mathbf{B}_{i,n_1+j} := \int_\Omega \frac{\partial \varphi_h^{(j)}}{\partial x_2}\ \psi_h^{(i)}\ d\mathbf{x},$$
$$1 \leqslant i \leqslant N_2,\ 1 \leqslant j \leqslant n_1.$$

We note that the matrices $\mathbf{M}_1$, $\mathbf{M}_3$, and $\mathbf{A}$ are symmetric and positive definite. In particular, there exist constants $\mu_1 > 0$, $\mu_3 > 0$, and $\alpha > 0$ such that for $\mathbf{v} \in \mathbb{R}^{N_1}$ and $\mathbf{Y} \in \mathbb{R}^{N_3}$ there holds

$$\mathbf{v}^T\mathbf{M}_1\mathbf{v} \geqslant \mu_1\|\mathbf{v}\|^2, \quad \mathbf{Y}^T\mathbf{M}_3\mathbf{Y} \geqslant \mu_3\|\mathbf{Y}\|^2, \quad \mathbf{v}^T\mathbf{A}\mathbf{v} \geqslant \alpha\|\mathbf{v}\|^2. \tag{2.14}$$

The matrix $\mathbf{B}^T$ satisfies an inf-sup condition, or equivalently

$$\|\mathbf{B}^T\mathbf{q}\|^2 \geqslant \beta\|\mathbf{q}\|^2_{\mathbb{R}^{N_2}\setminus\mathbb{R}^1}, \quad \beta > 0,\ \mathbf{q} \in \mathbb{R}^{N_2} \setminus \mathrm{span}\{(1,\ldots,1)^T\}. \tag{2.15}$$

We further define the nonlinear mappings $\mathbf{C} : \mathbb{R}^{N_1} \to \mathbb{R}^{N_1}$, $\mathbf{F} : \mathbb{R}^{N_3} \to \mathbb{R}^{N_1}$, and $\mathbf{K} : \mathbb{R}^{N_3} \to \mathbb{R}^{N_3 \times N_1}$ according to

$$(\mathbf{C}(\mathbf{u}))_{(\ell-1)n_1+i} := \sum_{j,k=1}^{n_1} \sum_{m=1}^{2} \rho \int_\Omega \varphi_h^{(i)} \varphi_h^{(j)} \frac{\partial \varphi_h^{(k)}}{\partial x_m} d\mathbf{x} u_{(m-1)n_1+j} u_{(\ell-1)n_1+k},$$

$$(\mathbf{F}(\mathbf{X}^{(k+1)}))_{(\ell-1)n_1+i} := \int_0^L \mathbf{f}_{h,\ell}^{(k+1)}(q) \varphi_h^{(i)}(\mathbf{X}_h^{(k+1)})dq,$$

where $1 \leqslant \ell \leqslant 2, 1 \leqslant i \leqslant n_1$, and

$$(\mathbf{K}(\mathbf{X}^{(k+1)}))_{(\ell-1)n_3+i,(\ell-1)n_1+j} := \int_0^L \varphi_h^{(j)}\left(\mathbf{X}_h^{(k+1)}\right)\chi_h^{(i)}dq.$$

(and zero else), where $1 \leqslant \ell \leqslant 2, 1 \leqslant i \leqslant n_3, 1 \leqslant j \leqslant n_1$, and $\mathbf{X}_h^{(k+1)} := (\sum_{i=1}^{n_3} X_i\chi_h^{(i)}, \sum_{i=1}^{n_3} X_{n_3+i}\chi_h^{(i)})^T$.

For $\mathbf{z} = (\mathbf{u}, \mathbf{p}, \mathbf{X})^T \in \mathbb{R}^{N_1+N_2+N_3}$ let us define the nonlinear function $\mathbf{H} : \mathbb{R}^N \to \mathbb{R}^N$, $N := N_1 + N_2 + N_3$, by

$$\mathbf{H}(\mathbf{z}) := -\begin{pmatrix} (\mathbf{A}+\mathbf{C}(\mathbf{u}))\mathbf{u} + \mathbf{B}^T\mathbf{p} - \mathbf{F}(\mathbf{X}) - \mathbf{F}_0 \\ \mathbf{B}\mathbf{u} - \mathbf{b} \\ -\mathbf{K}(\mathbf{X})\mathbf{u} \end{pmatrix} \in \mathbb{R}^N. \tag{2.16}$$

Note that the first two lines in (2.16) describe the finite element discretized stationary incompressible Navier–Stokes equations and that the vectors $\mathbf{F}_0 \in \mathbb{R}^{N_1}$ and $\mathbf{b} \in \mathbb{R}^{N_2}$ result from the inhomogeneous boundary data on Σ_{in} and Σ_{out}. We remind that the third line in (2.16) stems from the variational form of the equations of motion for the immersed boundary.

Denoting by $\mathbf{M} = \mathbf{blockdiag}(\mathbf{M}_1, \mathbf{0}, \mathbf{M}_3) \in \mathbb{R}^{N\times N}$ the (singular) mass matrix associated with ($\mathbf{u}_h$, $\mathbf{0}$, $\mathbf{X}_h$), the ODE describing the dynamics of the immersed boundary–fluid interaction can be written as

$$\begin{aligned} &\mathbf{M}\dot{\mathbf{z}}(t) = \mathbf{H}(\mathbf{z}(t)), \ t \in [0,T] \\ &\mathbf{z}(0) = \mathbf{z}_0, \end{aligned}$$

which is equivalent to the formulation as a Volterra equation of the second kind

$$\mathbf{0} = \mathbf{M}\mathbf{z}(t) - \mathbf{M}\mathbf{z}_0 - \int_0^t \mathbf{H}(\mathbf{z}(s))ds =: \widetilde{\mathbf{G}}(\mathbf{z}(t); t). \tag{2.17}$$

This represents a parameter-dependent nonlinear system of equations with trajectory $\{\mathbf{z}(t) | t \in [0,T]\}$. The numerical solution by means of Newton's method is not suitable, since it would require some *global* information of the Jacobian $\mathbf{H}'(\mathbf{z}(\cdot))$ up to the point $\mathbf{z}(t)$ and, in addition, an exact evaluation of the integral in (2.17).

To overcome these difficulties, we approximate (2.17) by the backward Euler (BE) scheme

$$\mathbf{0} = \mathbf{M}\mathbf{z}(t_{k+1}) - \mathbf{M}\mathbf{z}_k - \tau_k\mathbf{H}(\mathbf{z}(t_{k+1})), \ k \geqslant 0,$$

where $\tau_k := t_{k+1} - t_k$, i.e., for each time step we have to compute the root $\mathbf{z}(t_{k+1})$ of the nonlinear function

$$\mathbf{G}(\mathbf{z}; t_k + \tau_k) := \mathbf{M}\mathbf{z} - \mathbf{M}\mathbf{z}(t_k) - \tau_k\mathbf{H}(\mathbf{z}). \tag{2.18}$$

Consequently, the problem we deal with is a time-discretized approximation of a parameter-dependent nonlinear system of equations, and thus can be solved by the methodology presented in Section 3.

Setting $\mathbf{z}^{(k)} := (\mathbf{u}^{(k)}, \mathbf{p}^{(k)}, \mathbf{X}^{(k)})^T$, $0 \leqslant k \leqslant M$, at each time step the BE/BE FE-IB then amounts to the computation of $\mathbf{z}^{(k+1)}$, $0 \leqslant k \leqslant M-1$, as the solution of the nonlinear system

$$\mathbf{G}(\mathbf{z}^{(k+1)}; t_{k+1}) = \mathbf{0}, \tag{2.19}$$

where the nonlinear mapping $\mathbf{G}(\cdot; t_{k+1}) : \mathbb{R}^N \to \mathbb{R}^N$ *relative to* (τ_k,$\mathbf{z}(t_k)$) is given by

$$\mathbf{G}(\mathbf{z}; t_{k+1}) := \begin{pmatrix} (\mathbf{M}_1 + \tau_k\mathbf{A})\mathbf{u} + \tau_k\mathbf{C}(\mathbf{u}) + \tau_k\mathbf{B}^T\mathbf{p} - \tau_k\mathbf{F}(\mathbf{X}) - \mathbf{M}_1\mathbf{u}^{(k)} - \tau_k\mathbf{F}_0 \\ \mathbf{B}\mathbf{u} - \mathbf{b} \\ \mathbf{M}_3\mathbf{X} - \mathbf{M}_3\mathbf{X}^{(k)} - \tau_k\mathbf{K}(\mathbf{X})\mathbf{u} \end{pmatrix}, \tag{2.20}$$

where for scaling reasons we have multiplied the second block row by $1/\tau_k$. The Jacobian $\mathbf{G}'(\mathbf{z}; t_{k+1}) \in \mathbb{R}^{N\times N}$ reads as follows:

$$\mathbf{G}'(\mathbf{z}; t_{k+1}) := \begin{pmatrix} \mathbf{M}_1 + \tau_k\mathbf{A} + \tau_k\mathbf{C}'(\mathbf{u}) & \tau_k\mathbf{B}^T & -\tau_k\mathbf{F}'(\mathbf{X}) \\ \mathbf{B} & \mathbf{0} & \mathbf{0} \\ -\tau_k\mathbf{K}(\mathbf{X}) & \mathbf{0} & \mathbf{M}_3 - \tau_k\mathbf{K}'_{\mathbf{X}}(\mathbf{X}, \mathbf{u}) \end{pmatrix}. \tag{2.21}$$

Here, $\mathbf{C}'(\mathbf{u}) \in \mathbb{R}^{N_1\times N_1}$ and $\mathbf{F}'(\mathbf{X}) \in \mathbb{R}^{N_1\times N_3}$ are the Fréchet derivatives of $\mathbf{C}$ and $\mathbf{F}$ at $\mathbf{u}$ and $\mathbf{X}$, respectively, whereas $\mathbf{K}'_{\mathbf{X}}(\mathbf{X}, \mathbf{u}) \in \mathbb{R}^{N_3\times N_3}$ stands for the partial Fréchet derivative of $\mathbf{K}(\mathbf{X})\mathbf{u}$ with respect to $\mathbf{X}$ at ($\mathbf{X}$,$\mathbf{u}$).

Remark 2.4. We note that for the numerical evaluation of the Jacobians, the derivatives have been computed by automatic differentiation using the code *INTLAB* from [37].

The solution of the BE/BE FE-IB by a predictor–corrector continuation strategy in time requires the invertibility of the Jacobian which can be guaranteed under some restriction of the time step size.

Theorem 2.5. *For a given* $\mathbf{z} \in \mathbb{R}^N$ *and* $\tau^{min} > 0$, *assume that the time step size* τ_k *satisfies*

$$0 < \tau^{\min} \leqslant \tau_k \leqslant \tau_k^{\max}(\mathbf{z}) \;:=\; \min(\lambda_1, \lambda_2), \tag{2.22}$$
$$\lambda_1 \;:=\; -\frac{c_1}{c_2} + \sqrt{\frac{\mu_1}{2c_2} + \left(\frac{c_1}{c_2}\right)^2}, \quad \lambda_2 \;:=\; -\frac{d_1}{d_2} + \sqrt{\frac{\mu_3}{2d_2} + \left(\frac{d_1}{d_2}\right)^2},$$

where $c_\nu, d_\nu, 1 \leqslant \nu \leqslant 2$, depend on $\mathbf{z}$ and are given by

$$c_1 \;:=\; \|\mathbf{C}'(\mathbf{u})\| + \frac{1}{2}\|\mathbf{F}'(\mathbf{X})\| + \frac{1}{4}\|\mathbf{K}(\mathbf{X})\|^2/\|\mathbf{M}_1\|^2 - \alpha, \tag{2.23a}$$
$$c_2 \;:=\; 3\mu_1\Big(\|\mathbf{A}\|^2 + \|\mathbf{C}'(\mathbf{u})\|^2\Big), \tag{2.23b}$$
$$d_1 \;:=\; \frac{1}{2}\left(\|\mathbf{M}_1\|^2\|\mathbf{F}'(\mathbf{X})\| + \frac{1}{2}\|\mathbf{K}(\mathbf{X})\| + \|\mathbf{K}'_{\mathbf{X}}(\mathbf{X},\mathbf{u})\|\right), \tag{2.23c}$$
$$d_2 \;:=\; 3\mu_1\|\mathbf{F}'(\mathbf{X})\|^2. \tag{2.23d}$$

Then, the Jacobian $\mathbf{G}'(\mathbf{z}; t_{k+1}) \in \mathbb{R}^{N\times N}$ is invertible. In particular, there holds

$$\|(\mathbf{G}'(\mathbf{z}; t_{k+1}))^{-1}\| \leqslant \gamma^{-1}, \quad \gamma = \gamma(\mathbf{z}) \;:=\; \frac{\kappa_1}{\kappa_2}, \tag{2.24}$$
$$\kappa_1 \;:=\; \frac{1}{2}\min(\mu_1\|\mathbf{M}_1\|^2, \frac{3}{4}(\tau^{\min})^2\beta\mu_1, \mu_3),$$
$$\kappa_2 \;:=\; \left(\max(8\|\mathbf{M}_1\|^4 + 2\|\mathbf{B}\|^2, (\tau_k^{\max})^2\left(8\|\mathbf{M}_1\|^4 + \frac{\mu_1^2}{2}\|\mathbf{B}^T\|^2\right), 1)\right)^{1/2}.$$

Proof. For $\mathbf{w} = (\mathbf{v}, \mathbf{q}, \mathbf{Y})^T$ we choose $\bar{\mathbf{w}} = (\bar{\mathbf{v}}, \bar{\mathbf{q}}, \overline{\mathbf{Y}})^T$ according to $\bar{\mathbf{v}} = 2\|\mathbf{M}_1\|^2\mathbf{v} + \mu_1\tau_k\mathbf{B}^T\mathbf{q}/2, \bar{\mathbf{q}} = \mathbf{B}\mathbf{v} - 2\tau_k\|\mathbf{M}_1\|^2\mathbf{q}$, and $\overline{\mathbf{Y}} = \mathbf{Y}$. It follows that

$$\begin{aligned}\bar{\mathbf{w}}^T G'(\mathbf{z}; t_{k+1})\mathbf{w} = &\left(2\|\mathbf{M}_1\|^2\mathbf{v} + \frac{1}{2}\mu_1\tau_k\mathbf{B}^T\mathbf{q}\right)^T(\mathbf{M}_1 + \tau_k\mathbf{A} + \tau_k\mathbf{C}'(\mathbf{u}))\mathbf{v}\\ &+ \tau_k\left(2\|\mathbf{M}_1\|^2\mathbf{v} + \frac{1}{2}\mu_1\tau_k\mathbf{B}^T\mathbf{q}\right)^T\mathbf{B}^T\mathbf{q} - \tau_k\left(2\|\mathbf{M}_1\|^2\mathbf{v} + \frac{1}{2}\mu_1\tau_k\mathbf{B}^T\mathbf{q}\right)^T\mathbf{F}'(\mathbf{X})\mathbf{Y}\\ &+ (\mathbf{B}\mathbf{v} - 2\tau_k\|\mathbf{M}_1\|^2\mathbf{q})^T\mathbf{B}\mathbf{v} - \tau_k\mathbf{Y}^T\mathbf{K}(\mathbf{X})\mathbf{v} + \mathbf{Y}^T(\mathbf{M}_3 - \tau_k\mathbf{K}'_{\mathbf{X}}(\mathbf{X},\mathbf{u}))\mathbf{Y}.\end{aligned} \tag{2.25}$$

For the first term on the right-hand side in (2.25) we obtain

$$\begin{aligned}\left(2\|\mathbf{M}_1\|^2\mathbf{v} + \frac{1}{2}\mu_1\tau_k\mathbf{B}^T\mathbf{q}\right)^T(\mathbf{M}_1 + \tau_k\mathbf{A} + \tau_k\mathbf{C}'(\mathbf{u}))\mathbf{v} = 2\|\mathbf{M}_1\|^2\mathbf{v}^T(\mathbf{M}_1 + \tau_k\mathbf{A} + \tau_k\mathbf{C}'(\mathbf{u}))\mathbf{v} + \frac{1}{2}\mu_1\tau_k(\mathbf{B}^T\mathbf{q})^T(\mathbf{M}_1 + \tau_k\mathbf{A}\\ + \tau_k\mathbf{C}'(\mathbf{u}))\mathbf{v}.\end{aligned} \tag{2.26}$$

Using (2.14), the first term on the right-hand side in (2.26) can be estimated from below as follows

$$2\|\mathbf{M}_1\|^2\mathbf{v}^T(\mathbf{M}_1 + \tau_k\,\mathbf{A} + \tau_k\mathbf{C}'(\mathbf{u}))\,\mathbf{v} \geqslant 2\|\mathbf{M}_1\|^2\underbrace{\mathbf{v}^T\mathbf{M}_1\mathbf{v}}_{\geqslant\mu_1\|\mathbf{v}\|^2} + 2\tau_k\|\mathbf{M}_1\|^2\underbrace{\mathbf{v}^T\mathbf{A}\mathbf{v}}_{\geqslant\alpha\|\mathbf{v}\|^2} - 2\tau_k\|\mathbf{M}_1\|^2\|\mathbf{C}'(\mathbf{u})\|\|\mathbf{v}\|^2. \tag{2.27}$$

Using Young's inequality, the second term on the right-hand side in (2.26) can be estimated from above according to

$$\begin{aligned}\frac{1}{2}\mu_1\tau_k(\mathbf{B}^T\mathbf{q})^T(\mathbf{M}_1 + \tau_k\mathbf{A} + \tau_k\mathbf{C}'(\mathbf{u}))\mathbf{v} &\leqslant \frac{\sqrt{\mu_1}}{\sqrt{2}}\|\mathbf{M}_1\|\|\mathbf{v}\|\frac{\sqrt{\mu_1}}{\sqrt{2}}\tau_k\|\mathbf{B}^T\mathbf{q}\| + \tau_k^2\frac{\mu_1}{2}\|\mathbf{A}\|\|\mathbf{v}\|\|\mathbf{B}^T\mathbf{q}\| + \tau_k^2\frac{\mu_1}{2}\|\mathbf{C}'(\mathbf{u})\|\|\mathbf{v}\|\|\mathbf{B}^T\mathbf{q}\|\\ &\leqslant \frac{1}{8}\frac{\mu_1}{2}\tau_k^2\|\mathbf{B}^T\mathbf{q}\|^2 + 2\frac{\mu_1}{2}\|\mathbf{M}_1\|^2\|\mathbf{v}\|^2 + \frac{1}{24}\frac{\mu_1}{2}\tau_k^2\|\mathbf{B}^T\mathbf{q}\|^2 + 6\frac{\mu_1}{2}\tau_k^2\|\mathbf{A}\|^2\|\mathbf{v}\|^2 + \frac{1}{24}\frac{\mu_1}{2}\tau_k^2\|\mathbf{B}^T\mathbf{q}\|^2 + 6\frac{\mu_1}{2}\tau_k^2\|\mathbf{C}'(\mathbf{u})\|^2\|\mathbf{v}\|^2.\end{aligned} \tag{2.28}$$

For the second term on the right-hand side in (2.25) it follows that

$$\tau_k\left(2\|\mathbf{M}_1\|^2\mathbf{v} + \frac{1}{2}\mu_1\tau_k\mathbf{B}^T\mathbf{q}\right)^T\mathbf{B}^T\mathbf{q} = 2\tau_k\|\mathbf{M}_1\|^2\mathbf{v}^T\mathbf{B}^T\mathbf{q} + \frac{\mu_1}{2}\tau_k^2\|\mathbf{B}^T\mathbf{q}\|^2. \tag{2.29}$$

Another application of Young's inequality reveals that the third term on the right-hand side in (2.26) can be estimated from above by means of

$$\begin{aligned}\tau_k\left(2\|\mathbf{M}_1\|^2\mathbf{v} + \frac{1}{2}\mu_1\tau_k\mathbf{B}^T\mathbf{q}\right)^T\mathbf{F}'(\mathbf{X})\mathbf{Y} = 2\tau_k\|\mathbf{M}_1\|^2\mathbf{v}^T\mathbf{F}'(\mathbf{X})\mathbf{Y} + \frac{\mu_1}{2}\tau_k^2(\mathbf{B}^T\mathbf{q})^T\mathbf{F}'(\mathbf{X})\mathbf{Y} \leqslant \tau_k\|\mathbf{M}_1\|^2\|\mathbf{F}'(\mathbf{X})\|(\|\mathbf{v}\|^2 + \|\mathbf{Y}\|^2)\\ + \frac{1}{24}\frac{\mu_1}{2}\tau_k^2\|\mathbf{B}^T\mathbf{q}\|^2 + 6\frac{\mu_1}{2}\tau_k^2\|\mathbf{F}'(\mathbf{X})\|^2\|\mathbf{Y}\|^2.\end{aligned} \tag{2.30}$$

For the fourth term on the right-hand side in (2.26) we obtain

$$(\mathbf{Bv} - 2\tau_k\|\mathbf{M}_1\|^2\mathbf{q})^T\ \mathbf{Bv} = \underbrace{\|\mathbf{Bv}\|^2}_{\geqslant 0} - 2\tau_k\|\mathbf{M}_1\|^2\mathbf{q}^T\mathbf{Bv}. \tag{2.31}$$

Using Young's inequality again, the fifth term on the right-hand side in (2.26) can be estimated from above as follows

$$\tau_k\mathbf{Y}^T\mathbf{K}(\mathbf{X})\mathbf{v} \leqslant \frac{1}{2}\tau_k\|\mathbf{K}(\mathbf{X})\|(\|\mathbf{v}\|^2 + \|\mathbf{Y}\|^2). \tag{2.32}$$

Finally, in view of (2.14), for the sixth term on the right-hand side in (2.26) we get the lower bound

$$\big(\mathbf{M}_3 - \tau_k\mathbf{K}'_{\mathbf{X}}(\mathbf{X},\mathbf{u})\big)\mathbf{Y} \geqslant \underbrace{\mathbf{Y}^T\mathbf{M}_3\mathbf{Y}}_{\geqslant \mu_3\|\mathbf{Y}\|^2} - \tau_k\|\mathbf{K}'_{\mathbf{X}}(\mathbf{X},\mathbf{u})\|\|\mathbf{Y}\|^2. \tag{2.33}$$

Summarizing (2.26)–(2.33), from (2.25) we deduce

$$\bar{\mathbf{w}}^T G'(\mathbf{z};t_{k+1})\mathbf{w} \geqslant \|\mathbf{M}_1\|^2(\mu_1 - 2c_1\tau_k - c_2\tau_k^2)\|\mathbf{v}\|^2 + \frac{3}{8}\tau_k^2\mu_1\|\mathbf{B}^T\mathbf{q}\|^2 + (\mu_3 - 2d_1\tau_k - d_2\tau_k^2)\|\mathbf{Y}\|^2. \tag{2.34}$$

We choose τ_k such that

$$\mu_1 - 2c_1\tau_k - c_2\tau_k^2 \geqslant \frac{1}{2}\mu_1, \quad \mu_3 - 2d_1\tau_k - d_2\tau_k^2 \geqslant \frac{1}{2}\mu_3, \tag{2.35}$$

which is satisfied, if τ_k obeys the upper bound in (2.22). On the other hand, using (2.15) and the lower bound in (2.22), it follows that

$$\frac{3}{8}\tau_k^2\mu_1\|\mathbf{B}^T\mathbf{q}\|^2 \geqslant \frac{3}{8}(\tau_k^{(min)})^2\beta\mu_1\|\mathbf{q}\|^2_{\mathbb{R}^{N_2}\setminus\mathbb{R}^1}. \tag{2.36}$$

Taking advantage of (2.35) and (2.36) in (2.34), we finally obtain

$$\bar{\mathbf{w}}^T G'(\mathbf{z};t_{k+1})\mathbf{w} \geqslant \kappa_1\|\mathbf{w}\|^2.$$

Consequently, in view of

$$\|\bar{\mathbf{w}}\| \leqslant \kappa_2\|\mathbf{w}\|,$$

$\mathbf{G}'(\mathbf{z};t_{k+1})$ satisfies the inf-sup condition

$$\inf_{\mathbf{w}\neq 0}\sup_{\hat{\mathbf{w}}\neq 0}\frac{\hat{\mathbf{w}}^T\mathbf{G}'(\mathbf{z};t_{k+1})\mathbf{w}}{\|\mathbf{w}\|\|\hat{\mathbf{w}}\|} \geqslant \inf_{\mathbf{w}\neq 0}\frac{\bar{\mathbf{w}}^T\mathbf{G}'(\mathbf{z};t_{k+1})\mathbf{w}}{\|\mathbf{w}\|\|\bar{\mathbf{w}}\|} \geqslant \gamma,$$

from which we deduce bijectivity by means of the generalized Lax–Milgram lemma (cf., e.g., [12,13]). □

Remark 2.6. We may expect a time step restriction, if the convective term and/or the deformation of the particle is dominant, i.e., in case $\|\mathbf{C}'(\mathbf{u})\|$ and/or $\|\mathbf{F}'(\mathbf{X})\|$ is large. These scenarios are reflected by the time step restriction (2.22).

Usually, the step size restriction (2.22) is relatively mild and *not* the reason why we use an adaptive continuation strategy. The adaptivity is due to the convergence requirements of the Newton correction scheme, as explained below.

3. Adaptive Newton continuation

When it comes to the numerical solution of (2.19) by means of the ordinary Newton method

$$\mathbf{G}'(\mathbf{z}^{(\ell)};t_{k+1})\ \Delta\mathbf{z}^{(\ell)} = -\mathbf{G}(\mathbf{z}^{(\ell)};t_{k+1}), \tag{3.1a}$$

$$\mathbf{z}^{(\ell+1)} = \mathbf{z}^{(\ell)} + \Delta\mathbf{z}^{(\ell)}, \tag{3.1b}$$

it turns out that its naive application is seldom successful. The reason is that the IB scheme is typically badly conditioned in the sense that even small perturbations of $\mathbf{X}$ from its target position (here: $\mathbf{X}(t_{k+1})$) cause strong counterforces that lead to rapid oscillations in all unknowns resulting in non-convergence of (3.1a), (3.1b). A remedy for this problem is to use a modified Newton method with adaptively chosen damping parameters (step lengths) $\alpha_\ell \in [\alpha_{\min},1]$ for the update $\mathbf{z}^{(\ell+1)} = \mathbf{z}^{(\ell)} + \alpha_\ell\Delta\mathbf{z}^{(\ell)}$. More precisely, we use the algorithm `NLEQ-ERR` from [15] which employs a combination of damped ordinary and simplified Newton steps in order to build certain contraction factors serving as convergence monitoring quantities (for details, see [15] and below). The actual motivation for this algorithm is that it can be used in the context of parameter-dependent nonlinear problems.

Our approach is based on the affine invariant convergence theory for Newton-like methods developed in [15] and updates the time parameter t in an adaptive way using local information about the trajectory $\{\mathbf{z}(t) = (\mathbf{u}(t), \mathbf{p}(t), \mathbf{X}(t)) | t \in [0,T]\}$. We

follow this trajectory in a predictor–corrector manner. For the computation of the prediction step it is essential how to choose the increment τ_k, since this is closely related to the problem of staying inside the Kantorovich neighborhood of the solution at time $t_k + \tau_k$. Predictor–corrector methods can be seen as discrete continuation methods where the continuation step plays the role of a prediction step. Consider a parameter-dependent nonlinear system

$$\mathbf{G}(\mathbf{z};t) = \mathbf{0}, \quad t \in [0,T],\ \mathbf{z} \in \mathbb{R}^N, \tag{3.2}$$

where $\mathbf{G}(\cdot;t) : \mathbb{R}^N \to \mathbb{R}^N$and assume that there exists a solution $\mathbf{z}(t) \in \mathbb{R}^N$ for $t \in [0,T]$. Discrete continuation methods solve (3.2) with respect to a partitioning $t_0 < t_1 < \cdots < t_M = T$, $M > 1$, of the interval $[0,T]$. This partitioning is not given in advance, but computed adaptively during the solution process. In order to solve the subproblems (2.19) successively by a Newton solver, we need sufficiently good initial guesses $\hat{\mathbf{z}}^{(0)}(t_{k+1})$ which have to be provided by a continuation step. It has to be adapted in such a way that the convergence requirements of the subsequent correction step (2.19) are met. The quality of approximation of the prediction can be controlled by two factors, the steplength τ_k and the type of continuation. The simplest possible choice for a continuation step $\mathbf{z}(t_k) \to \hat{\mathbf{z}}(t_{k+1})$ is constant continuation, i.e.,

$$\hat{\mathbf{z}}(t_{k+1}) := \mathbf{z}(t_k), \tag{3.3}$$

also called classical continuation. It involves no further computations and for simplicity, we will stick to this choice. By Taylor expansion, we get as approximation error

$$\|\hat{\mathbf{z}}(t_k + \tau_k) - \mathbf{z}(t_k + \tau_k)\| \leqslant \eta\tau_k. \tag{3.4}$$

We remark that the constant $\eta = \max_{t\in[0,T]}\|\dot{z}(t)\|$ is a key quantity for an adaptive stepsize selection. It will be used below.

The term affine covariance means that the Newton iterates $\mathbf{z}^{(\ell)}$ are invariant with respect to affine transformations $\mathbf{G} \to \mathbf{TG}$ of the image space of $\mathbf{G}$ by a regular matrix $\mathbf{T}$, which can be easily seen. Invariance with respect to affine transformations of the domain space is referred to as affine contravariance. Both are subtopics to the generic term affine invariance. We encounter affine covariance in Lipschitz conditions like

$$\|(\mathbf{G}'(\mathbf{z}_1;t_{k+1}))^{-1}\ (\mathbf{G}(\mathbf{z}_1;t_{k+1}) - \mathbf{G}(\mathbf{z}_2;t_{k+1}))\| \leqslant \omega\|\mathbf{z}_1 - \mathbf{z}_2\|$$

through its affine covariant constant. They appear in certain affine covariant Newton convergence theorems (see Theorem 3.1 below). By nature of the affine covariant concept, such theorems can only be about the iterates' increments $\mathbf{\Delta z}^{(\ell)}$ or errors $\mathbf{z}^{(\ell)} - \mathbf{z}^*$, not about residuals $\mathbf{G}(\mathbf{z}^{(\ell)};t_{k+1})$. This has to be taken into account in the subalgorithms of an algorithmic realization of a discrete continuation method formulated in affine covariant terms.

In our case, the object of interest is the homotopy path $\mathbf{z}(t)$ which lives in the domain of the mapping $\mathbf{G}$. Therefore, the concept of affine covariance is the adequate framework.

We consider a convergence analysis of the simplified Newton method which is most appropriate to derive steplength criteria for a discrete continuation method. We recall that for a given start iterate $\mathbf{z}^{(0)}$ the simplified Newton method is of the form

$$\mathbf{G}'(\mathbf{z}^{(0)};t_{k+1})\ \overline{\mathbf{\Delta z}}^{(\ell)} = -\mathbf{G}(\mathbf{z}^{(\ell)};t_{k+1}), \tag{3.5a}$$

$$\mathbf{z}^{(\ell+1)} = \mathbf{z}^{(\ell)} + \overline{\mathbf{\Delta z}}^{(\ell)}, \ell = 0,1,\ldots. \tag{3.5b}$$

It is characterized by the fixed Jacobian $\mathbf{G}'(\mathbf{z}^{(0)};t_{k+1})$ which is used for all iterations. We cite the following affine covariant convergence result (cf. Theorem 2.5) in [15]):

Theorem 3.1. *Let $D \subset \mathbb{R}^N$ be open and convex, $\mathbf{G} : D \to \mathbb{R}^N$ be continuously differentiable, and $\mathbf{z}^{(0)} \in D$ such that $\mathbf{G}'(\mathbf{z}^{(0)})$ is invertible. Further, for some $\omega > 0$ let the affine covariant Lipschitz condition*

$$\|(\mathbf{G}'(\mathbf{z}^{(0)}))^{-1}(\mathbf{G}'(\mathbf{z}) - \mathbf{G}'(\mathbf{z}^{(0)}))\| \leqslant \omega\|\mathbf{z} - \mathbf{z}^{(0)}\|, \mathbf{z} \in D, \tag{3.6}$$

hold true. Assume further

$$h_0 := \omega\|\overline{\mathbf{\Delta z}}^{(0)}\| \leqslant \frac{1}{2} \tag{3.7}$$

and define $\delta^* := 1 - \sqrt{1-2h_0}, \rho := \delta^*/\omega$. Suppose that the closed ball $\overline{B_\rho(\mathbf{z}^{(0)})}$ is contained in D. Then, the simplified Newton method (3.5b) generates iterates $\{\mathbf{z}^{(\ell)}\}_{\ell\in\mathbb{N}} \subset \overline{B_\rho(\mathbf{z}^{(0)})}$ converging to $\mathbf{z}^*$ with $\mathbf{G}(\mathbf{z}^*) = 0$, and there holds the estimate

$$\frac{\|\mathbf{z}^{(\ell+1)} - \mathbf{z}^{(\ell)}\|}{\|\mathbf{z}^{(\ell)} - \mathbf{z}^{(\ell-1)}\|} \leqslant \frac{1}{2}(\delta_\ell + \delta_{\ell-1}), \quad \ell \geqslant 1, \tag{3.8}$$

where $\delta_0 := 0$ and $\delta_{\ell+1} := h_0 + 1/2\delta_\ell^2$, $\ell \geqslant 0$.

The contraction factors

$$\Theta_\ell := \frac{\|\overline{\mathbf{\Delta z}}^{(\ell+1)}\|}{\|\overline{\mathbf{\Delta z}}^{(\ell)}\|}, \ell \geqslant 0, \tag{3.9}$$

serve as monitoring quantities in Newton algorithms: From the convergence rate estimate (3.8) it follows that $\Theta_\ell \leqslant 1/2\,(\delta_{\ell+1}+\delta_\ell)$, $\ell \geqslant 0$. Along with $\delta_0 = 0$, $\delta_1 = h_0$ and the definition of h_0 from (3.7), we get

$$\Theta_0 \leqslant \frac{1}{2}\omega\|\overline{\Delta \mathbf{z}}^{(0)}\|. \tag{3.10}$$

This estimate is equivalent to

$$\frac{2\Theta_0}{\|\overline{\Delta \mathbf{z}}^{(0)}\|} \leqslant \omega, \tag{3.11}$$

which provides a lower bound for ω respectively the local Lipschitz constant $\hat{\omega}$ (cf. Theorem 3.2 below). Along with η from (3.4), this is the second key quantity for an adaptive step size selection strategy. In the following, we have to assume that $\tau \geqslant \tau^{\min}$ for some given $\tau^{\min} > 0$ to guarantee boundedness of γ^{-1} (cf. (2.24)). This is in agreement with the algorithmic realization of the predictor–corrector scheme (see Algorithm 3.6 below) where the case $\tau_k < \tau^{\min}$ serves as a convergence failure criterion.

Theorem 3.2. *Let $\mathbf{G}'(\mathbf{z};t)$ be nonsingular for all $(\mathbf{z};t) \in D \times [0,T]$, assume that the homotopy path $\mathbf{z}:[0,T] \to D$ exists, and let $t_k \in [0,T]$. Further, suppose that there exists a local Lipschitz constant $\hat{\omega}$ such that for all $\mathbf{z} \in D$ and for all $0 < \tau^{min} \leqslant \tau \leqslant T - t_k$ satisfying $\hat{\mathbf{z}}(t_k+\tau) \in D$, the affine covariant Lipschitz condition*

$$\|(\mathbf{G}'(\hat{\mathbf{z}}(t_k+\tau);t_k+\tau))^{-1}(\mathbf{G}'(\mathbf{z};t_k+\tau) - \mathbf{G}'(\hat{\mathbf{z}}(t_k+\tau);t_k+\tau))\| \leqslant \hat{\omega}\|\mathbf{z} - \hat{\mathbf{z}}(t_k+\tau)\| \tag{3.12}$$

holds true. Then, the simplified Newton method (3.5b) with starting point $\hat{\mathbf{z}}(t_k+\tau) := z(t_k)$ (classical continuation) converges towards the solution $\mathbf{z}(t_k+\tau)$ for all stepsizes

$$\tau^{\min} \leqslant \tau \leqslant \tau^{\max}(t_k) := \frac{\sqrt{2}-1}{\hat{\omega}\eta}. \tag{3.13}$$

Proof. For completeness we present the proof from Corollary 5.5 in [15], since we will use an estimate from the proof for the subsequent discussion. For the application of Theorem 3.1 we need

$$\hat{\omega}\|\overline{\Delta \mathbf{z}}^{(0)}(t_k+\tau)\| \leqslant \frac{1}{2}. \tag{3.14}$$

To this end, we derive an upper bound $r(\tau)$ for $\|\overline{\Delta \mathbf{z}}^{(0)}\|$. We set $\hat{\mathbf{z}} := \hat{\mathbf{z}}(t_{k+1})$, $\mathbf{z} := \mathbf{z}(t_{k+1})$ and consider

$$\begin{aligned}
\|\overline{\Delta \mathbf{z}}^{(0)}(t_{k+1})\| &= \|(\mathbf{G}'(\hat{\mathbf{z}},t_{k+1}))^{-1}\ \mathbf{G}(\hat{\mathbf{z}},t_{k+1})\| = \left\|(\mathbf{G}'(\hat{\mathbf{z}};t_{k+1}))^{-1}\left(\mathbf{G}(\hat{\mathbf{z}};t_{k+1}) - \overbrace{\mathbf{G}(\mathbf{z};t_{k+1})}^{=\mathbf{0}}\right)\right\| \\
&= \|(\mathbf{G}'(\hat{\mathbf{z}},t_{k+1}))^{-1}\ \int_0^1 \mathbf{G}'(\mathbf{z}+s(\hat{\mathbf{z}}-\mathbf{z});t_{k+1})(\hat{\mathbf{z}}-\mathbf{z})\ ds\| \\
&= \left\|\int_0^1 (\mathbf{G}'(\hat{\mathbf{z}};t_{k+1}))^{-1}(\mathbf{G}'(\mathbf{z}+s\ (\hat{\mathbf{z}}-\mathbf{z}),t_{k+1}) \pm \mathbf{G}'(\hat{\mathbf{z}},t_{k+1}))\ (\hat{\mathbf{z}}-\mathbf{z})ds\right\| \\
&\leqslant \|\hat{\mathbf{z}}-\mathbf{z}\|\left(1 + \int_0^1 \|(\mathbf{G}'(\hat{\mathbf{z}};t_{k+1}))^{-1}\ (\mathbf{G}'(\mathbf{z}+s\ (\hat{\mathbf{z}}-\mathbf{z});t_{k+1}) - \mathbf{G}'(\hat{\mathbf{z}};t_{k+1}))\|\ ds\right) \\
&\overset{(3.12)}{\leqslant} \|\hat{\mathbf{z}}-\mathbf{z}\|\left(1 + \hat{\omega}\|\hat{\mathbf{z}}-\mathbf{z}\|\int_0^1 |1-s|ds\right).
\end{aligned}$$

From the definition of η (cf. (3.4)) we know $\|\hat{\mathbf{z}}(t_{k+1}) - \mathbf{z}(t_{k+1})\| \leqslant \eta\tau$, whence

$$\|\overline{\Delta \mathbf{z}}^{(0)}(t_k+\tau)\| \leqslant \eta\tau\left(1 + \frac{1}{2}\hat{\omega}\eta\tau\right) =: r(\tau). \tag{3.15}$$

The crucial step is to use this estimate for requirement (3.14) to arrive at

$$\hat{\omega}\eta\tau\left(1 + \frac{1}{2}\hat{\omega}\eta\tau\right) \leqslant \frac{1}{2},$$

which is fulfilled for $\hat{\omega}\eta\tau \leqslant \sqrt{2}-1$. Under this condition, which is equivalent to (3.13), Theorem 3.1 can be applied, and we conclude. □

Remark 3.3. According to Theorem 3.2, the iterates $\{\mathbf{z}^{(\ell)}\}_\ell$ stay within the closed ball $\overline{B_\rho(\hat{\mathbf{z}}^{(0)}(t_{k+1}))} \subset \overline{B_{1/\hat{\omega}}(\mathbf{z}(t_k))} =: B$, if the step size restriction (3.13) is fulfilled. (This is also true when, in practice, we use a combination of the ordinary and the simplified Newton method.) Hence, all Newton iterates are well defined, if in view of (2.22) we choose

$$\tau^{\min} \leqslant \tau_k \leqslant \min\ \left(\frac{\sqrt{2}-1}{\hat{\omega}\ \eta}, \min_{\mathbf{z}\in B}(\tau^{\max}(\mathbf{z})) \right).$$

Remark 3.4. We check the affine covariant Lipschitz condition (3.12) from Theorem 3.2 in case the nonlinear mapping $\mathbf{G}(\cdot; t_{k+1}),\ t_{k+1} = t_k + \tau,\ k \in \mathbb{N}_0$, is given by (2.20). Let $\tau \geqslant \tau^{\min} > 0$ as in Theorem 3.2. Setting for brevity $\hat{\mathbf{z}} := \hat{\mathbf{z}}(t_k + \tau)$, we have

$$\mathbf{G}'(\mathbf{z}; t_k + \tau) - \mathbf{G}'(\hat{\mathbf{z}}(t_k + \tau); t_k + \tau) = \begin{pmatrix} \tau(\mathbf{C}'(\mathbf{u}) - \mathbf{C}'(\hat{\mathbf{u}})) & \mathbf{0} & -\tau(\mathbf{F}'(\mathbf{X}) - \mathbf{F}'(\hat{\mathbf{X}})) \\ \mathbf{0} & \mathbf{0} & \mathbf{0} \\ -\tau(\mathbf{K}(\mathbf{X}) - \mathbf{K}(\hat{\mathbf{X}})) & \mathbf{0} & -\tau\Big(\mathbf{K}'_{\mathbf{X}}(\mathbf{X}, \mathbf{u}) - \mathbf{K}'_{\mathbf{X}}(\hat{\mathbf{X}}, \hat{\mathbf{u}})\Big) \end{pmatrix}.$$

We denote by $L_{\mathbf{C}'}$ the (local) Lipschitz constant $L_{\mathbf{C}'}(\mathbf{z}(t_k))$ of the Fréchet derivative $\mathbf{C}'$, i.e.,

$$\|\mathbf{C}'(\mathbf{u}) - \mathbf{C}'(\hat{\mathbf{u}})\| \leqslant L_{\mathbf{C}'} \|\mathbf{u} - \hat{\mathbf{u}}\|$$

and define $L_{\mathbf{F}'}, L_{\mathbf{K}}, L_{\mathbf{K}'_{\mathbf{X}}}$ similarly. Then, with $\gamma = \gamma(\mathbf{z}(t_k))$ and in view of (2.24), from Theorem 2.5 we obtain (3.12) with a τ-independent upper bound

$$\widehat{\Omega} \ := \ \gamma^{-1}\ (T - t_k)\ \max(L_{\mathbf{C}'}, L_{\mathbf{F}'}, L_{\mathbf{K}}, L_{\mathbf{K}'_{\mathbf{X}}}). \tag{3.16}$$

In view of (2.24), the quantity γ^{-1} depends on the choice of $\tau^{\min}$. On the other hand, according to (3.13) and (3.16), $\tau^{\min}$ determines an upper bound $(\sqrt{2}-1)/(\widehat{\Omega}\ \eta)$ for τ. The following result provides a condition under which the interval $[\tau^{\min}, \tau^{\max}(t_k)]$ is nonempty.

Lemma 3.1. *Assume that for*

$$\widehat{C}(\mathbf{z}(t_k), t_k)\ :=\ \frac{\sqrt{2}-1}{2\eta}\ \frac{1}{\max\left(L_{\mathbf{C}'}, L_{\mathbf{F}'}, L_{\mathbf{K}}, L_{\mathbf{K}'_{\mathbf{X}}}\right)(T - t_k)\kappa_2(\mathbf{z}(t_k))}, \tag{3.17}$$

the condition

$$\widehat{C}(\mathbf{z}(t_k), t_k)^2\, \frac{3}{4}\beta\mu_1 \min(\mu_1 \|M_1\|^2, \mu_3)\ \geqslant\ 1 \tag{3.18}$$

holds true. Then the interval $[\tau^{min}, \tau^{max}(t_k)]$ as in (3.13) is nonempty.

Proof. Observing (2.24), we introduce the quantities

$$K_1\ :=\ \widehat{C}(\mathbf{z}(t_k), t_k)\ \min(\mu_1 \|M_1\|^2, \mu_3), \quad K_2\ :=\ \widehat{C}(\mathbf{z}(t_k), t_k)\ \frac{3}{4}\beta\mu_1.$$

Since $\hat{\omega} \leqslant \widehat{\Omega}$, the interval $[\tau^{\min},\ \tau^{\max}(t_k)]$ with $\tau^{\max}(t_k) = \left(\sqrt{2}-1\right)/(\hat{\omega}\ \eta)]$ is nonempty, if

$$\tau^{\min} \leqslant \frac{\sqrt{2}-1}{\widehat{\Omega}\ \eta} = \min(K_1, K_2(\tau^{\min})^2) \tag{3.19}$$

holds true. In view of (3.18), we have $K_1 K_2 \geqslant 1$ and hence, we may choose $\tau^{\min}\ :=\ \sqrt{K_1/K_2}$ such that (3.19) is satisfied. □

The result of the last theorem has the drawback that it contains the unknown constants $\hat{\omega}$ and η. In order to exploit the steplength criterion (3.13) in an algorithmic realization, we use the following strategy:

We compute estimates $[\ \cdot\ ]$ of the a priori unknown constants and apply the steplength criterion with $\hat{\omega}$, η replaced with $[\hat{\omega}]$, $[\eta]$. By nature of the constants $\hat{\omega}$, η we have to work with lower bounds. Taking into account that both quantities appear in the denominator of (3.13), this strategy will in general overestimate the true maximal steplength $\tau^{\max}(t_k)$. Therefore, we only predict a maximal stepsize based on some estimates of the local constant $\hat{\omega}$ and the global constant η. It explains why we also need a correction formula for τ_k in case of convergence failure of the Newton corrector.

Remark 3.5. There is some ambiguity of the terms 'prediction' and 'correction', since we use each of them in two different meanings:

(a) in the context of a continuation method, we usually mean the prediction and the correction of the variable $\mathbf{z}$. Therefore, we use the expressions $\mathbf{z}$-prediction (by classical continuation) and $\mathbf{z}$-correction (by a Newton solver), respectively. For the continuation step in the $\mathbf{z}$-prediction,

(b) the steplength τ is predicted and, if necessary, corrected. We will address this as τ-prediction and τ-correction, respectively.

3.1. τ-Prediction strategy

We can use estimate (3.11) to obtain

$$\frac{2\Theta_0(t_k)}{\|\overline{\Delta\mathbf{z}}^{(0)}(t_k)\|} =: [\widehat{\omega}] \leqslant \hat{\omega}$$

as an estimate for $\hat{\omega}$ and likewise

$$\frac{\|\hat{\mathbf{z}}(t_k) - \mathbf{z}(t_k)\|}{\tau_{k-1}} =: [\eta] \leqslant \eta,$$

which obviously provides a lower bound of η due to (3.4). Inserting these estimates (which have the advantage of being computationally available) into (3.13) instead of $\hat{\omega}$ and η, results in the τ-prediction formula

$$\tau_k \;:=\; \tau_{k,0} \;:=\; [\tau^{\max}(t_k)] \;:=\; \frac{(\sqrt{2}-1)\|\Delta\mathbf{z}^{(0)}(t_k)\|}{2\Theta_0(t_k)\|\mathbf{z}^{(0)}(t_k) - \mathbf{z}(t_k)\|}\tau_{k-1}. \tag{3.20}$$

This formula predicts the next steplength τ_k adaptively based upon information about local and global constants of the homotopy gathered within the last Newton correction step. In (3.20) we have used the fact that the first increment of the simplified and the ordinary Newton method coincide. Since the exact solution $\mathbf{z}(t_k)$ is not known in general, we use the final solution of the Newton corrector as its replacement in (3.20) to obtain a computable expression. Due to the fact that this formula defines τ_k recursively, we need to specify some τ_0 for the first continuation step.

3.2. τ-Correction strategy

From (3.20) it is clear that $[\tau^{\max}(t_k)] \geqslant \tau^{\max}(t_k)$, and so the predicted steplength $\tau_k = \tau_{(k,0)}$ may be too large and could lead to a convergence failure of the Newton correction step. In this case, we need to correct it, i.e., $\tau_{(k,j+1)} \leftarrow \tau_{(k,j)}$ and repeat the last $\mathbf{z}$-prediction step, now with an adaptively reduced stepsize $\tau_{k,j+1}$. Here, we can deal with the quantity $\Theta_0(t_k + \tau_{(k,j)})$, since we have computed it in the last unsuccessful Newton correction at $t_k + \tau_{(k,j)}$. It can be exploited to gain refined information about the crucial quantity $\hat{\omega}\,\eta$ from (3.13): Estimate (3.10) in combination with (3.15) gives (using $t_{(k+1,j)} := t_k + \tau_{(k,j)}$):

$$\Theta_0(t_{(k+1,j)}) \leqslant \frac{1}{2}\hat{\omega}\eta\tau_{(k,j)}\left(1 + \frac{1}{2}\hat{\omega}\eta\tau_{(k,j)}\right).$$

Since $\hat{\omega}$, η, and $\tau_{(k,j)}$ are all nonnegative quantities, this is equivalent to

$$\hat{\omega}\eta\tau_{(k,j)} \geqslant \sqrt{4\Theta_0(t_{(k+1,j)}) + 1} - 1 \quad\Longleftrightarrow\quad \hat{\omega}\eta \geqslant \underbrace{\frac{\sqrt{4\Theta_0(t_{(k+1,j)}) + 1} - 1}{\tau_{(k,j)}}}_{=:[\hat{\omega}\eta]}.$$

Plugging this lower bound for $\hat{\omega}\eta$ into the stepsize formula (3.13), we obtain the τ-correction formula:

$$\tau_{(k,j+1)} \;:=\; [\tau^{\max}(t_k)] \;:=\; \frac{\sqrt{2}-1}{\sqrt{4\;\Theta_{\ell(j)}(t_{(k+1,j)}) + 1} - 1}\tau_{(k,j)},\; j \geqslant 0.$$

Here, Θ_0 has been replaced with $\Theta_{\ell(j)}$, where $\ell(j)$ stands for the ℓth Newton iteration (in the jth τ-correction cycle, $j \geqslant 0$) where convergence failure has occurred. This is not backed by rigorous theory but seems unavoidable and reasonable to get an executable algorithm:

Convergence failure for the simplified Newton method is accompanied by $\Theta_{\ell(j)} \geqslant 1$ (and nevertheless, if $\ell(j) \geqslant 1$ it is possible that $1/4 < \Theta_{0(j)} < 1$! $\Theta_0 \leqslant 1/4$ implies local convergence of the simplified Newton method, see (3.7) and (3.10)). Similarly, using the algorithm `NLEQ-ERR` as a Newton corrector, for convergence failure we must have $\Theta_{\ell(j)} \geqslant 1$. In both cases, for $\Theta_{\ell(j)} \geqslant 1$ we get an obvious reduction of the steplength, since

$$\frac{\sqrt{2}-1}{\sqrt{4\Theta_{\ell(j)}(t_{(k+1,j)}) + 1} - 1} \leqslant \frac{\sqrt{2}-1}{\sqrt{5}-1} \approx 0.34.$$

3.3. Adaptive continuation algorithm

We summarize the discussion about the time increment-adaptive prediction–correction scheme by the following pseudocode. The reader may concentrate, in particular, on the τ-prediction–correction for a clarification of the preceding discussion.

Algorithm 3.6. Adaptive predictor–corrector algorithm

% Initialization:
Specify the initial IB state variables $(\mathbf{u}^{(0)},\mathbf{p}^{(0)}, \mathbf{X}^{(0)}) =: \mathbf{z}(t_0)$ and a starting value $\tau_{(0,0)}$, bounds $\tau^{\min}$ and $\tau^{\max}$, and $\Theta_{\min} \ll 1$.
Set $t_0 := 0, k := 0$, and $j := 0$.
% Iteration:
`while` $t_k < T$
  $\%\mathbf{z}$ – *prediction step*:
  Set $t_{(k+1,j)} := t_k + \tau_{(k,j)}$
  Perform the classical continuation step $\hat{\mathbf{z}}^{(0)}(t_{(k+1,j)}) := \mathbf{z}(t_k)$
  $\%\mathbf{z}$ – *correction step*:
  Solve $\mathbf{G}(\mathbf{z};t_{(k+1,j)}) = 0$ with initial guess $\hat{\mathbf{z}}^{(0)}(t_{(k+1,j)})$ by the Newton solver `NLEQ-ERR`: Thereby, contraction factors $\Theta_\ell = \Theta_\ell(t_{(k+1,j)})$, $\ell \geqslant 0$, are computed and $\mathbf{z}$ gets updated by means of a damping factor α_ℓ according to $\hat{\mathbf{z}}^{(\ell+1)}(t_{(k+1,j)}) = \hat{\mathbf{z}}^{(\ell)}(t_{(k+1,j)}) + \alpha_\ell\ \Delta\mathbf{z}^{(\ell)}$.
  `if` Newton corrector was successful after $\ell = \ell(j) \geqslant 1$ iterations
    Set $t_{k+1} := t_{(k+1,j)}$
    Set $\mathbf{z}(t_{k+1}) := \hat{\mathbf{z}}^{(\ell)}(t_{(k+1,j)})$
    Set $\Theta_0 \leftarrow \max(\Theta_0, \Theta_{\min})$
    Predict the new time increment by

$$\tau_{(k+1,0)} := \frac{(\sqrt{2}-1)\|\Delta\mathbf{z}^{(0)}\|}{2\ \Theta_0\|\hat{\mathbf{z}}^{(0)}(t_{k+1}) - \mathbf{z}(t_{k+1})\|}\ \tau_{(k,j)}$$

    Set $\tau_{(k+1,0)} := \min(\tau_{(k+1,0)}, \tau^{\max})$
    `if` $\tau_{(k+1,0)} < \tau^{\min}$, stop: convergence failure `end`
  `else`
    Correct τ according to

$$\tau_{(k,j+1)} := \frac{\sqrt{2}-1}{\sqrt{4\ \Theta_{i(j)}(t_{(k+1,j)}) + 1} - 1}\,\tau_{(k,j)}$$

    `if` $\tau_{(k,j+1)} < \tau^{\min}$, stop: convergence failure `end`
    Set $j \leftarrow j + 1$ and go back to $\mathbf{z}$-prediction step
  `end`
  Set $j := 0$
  Set $k \leftarrow k + 1$
`end`

---

4. Numerical results

4.1. Motion of an RBC through a thin capillary

As an illustration of the adaptive continuation method we consider the motion and deformation of a red blood cell (RBC) immersed in an external microfluidic channel flow passing through a thin capillary. The plasma membrane of an RBC consists of a lipid bilayer membrane and an attached spectrin network as cytoskeleton [3]. Therefore, one might expect a rather complex fluidic behavior, since the underlying cytoskeleton can rearrange according to an external mechanical force [4]. However, it was demonstrated that lipid vesicles without an attached polymer network may serve as a simple model which already captures the basic physics of the fluid–structure interaction problem. We note that the dynamics of RBC and vesicles in fluid flow has been studied both experimentally (see [1,2,20,21,29,41]) and theoretically (cf. [6,7,22,24,35,38]). For the numerical study of the rheology of RBC in microchannels, the IB has been applied in [5,17,30,42], whereas the FE-IB has been used recently in [16]. It is well known that an RBC can pass through capillaries whose diameters are half or even less than the typical diameter of an RBC (7.5–8 μm), enabling oxygen supply also through highly branched blood vessels. We have considered a microchannel with a diameter varying between 20 and 4 μm, a density of $\rho = 1.0 \cdot 10^3$ kg/m^3, and a viscosity of $\eta = 6.0 \cdot 10^{-3}$ Pa · s both for the carrier fluid and the fluid enclosed by the membrane of the RBC. We have further assumed an inflow velocity of $g = 1.0 \cdot 10^{-2}$ m/s. Taking $d = 20$ μm as reference length, this results in a Reynolds number of $\mathcal{R}e \approx 3 \cdot 10^{-2}$, a typical magnitude for RBCs in microfluidic flows. We note that the maximal velocity inside the narrow part of the channel is almost five times higher than the inflow velocity which results in a strong deformation of the passing RBC whose elastic moduli have been chosen according to $\kappa_e = 6.0 \cdot 10^{-6}$ N/m and $\kappa_b = 2.0 \cdot 10^{-19}$ Nm (cf. [39]). In its initial state,

the RBC has a diameter of 7.8 μm and a perimeter of $L = 19.8$ μm. We have used a uniform finite element mesh for $\Omega = [0,50] \times [0,20] \backslash (17.5,32.5) \times ((0,8) \cup (12,20))$ μm^2 with mesh parameter $h = 1.0$ μm and a uniform partition of $[0,L]$, resulting in $N_1 + N_2 + N_3 = 10358 + 1340 + 114 = 11{,}812$. All computations have been performed under Linux on a work station featuring Intel Quad–CPU with 2.83 GHz each and 8 GB RAM.

We illustrate the difficulty associated with the semi-implicit BE/FE FE-IB from [16] by considering an RBC in a microchannel passing a thin capillary. The (constant) time step size was chosen too large, namely, $\tau = 1/250$, and oscillations in the IB state variables occurred leading to a 'torn apart' membrane. This is shown in Fig. 1. The same problem occurs even for $\tau = 1/350$ (see below).

In case of the fully implicit BE/BE FE-IB, the adaptively chosen time step sizes prevent from numerical instabilities. The adaptive step size selection algorithm detects the critical stage during the computation. This can be seen in Fig. 2 where τ_k gets clearly reduced (at approximately $t = 0.90$) and stays small as long as the RBC occupies the capillary. In the same figure, the evolution of the (scaled) potential energy $E_{\text{tot}}(t)$ of the membrane is displayed. An increase causes a reduction of τ_k and vice versa: when $E_{\text{tot}}(t)$ reaches its initial standard after leaving the thin capillary, τ is chosen larger again. The time instants of the snapshots of the RBC in Fig. 3 correspond to the markers in Fig. 2. It is noteworthy that the average time stepsize of the BE/BE FE-IB version is roughly 1/169. This means that the semi-implicit version with constant time steps $\tau = 1/350$ (see above) fails although its time increments are less than half of the average time step size of the fully implicit scheme. Moreover, in none of the 441 BE/BE FE-IB time steps it was necessary to perform a τ-correction, which seems to indicate that the τ-prediction mechanism is quite reliable.

The computation was stopped at $T = 2.61$ shortly before the RBC reached the outflow boundary. The computing time for the fully implicit BE/BE FE-IB with initial $\tau_{(0,0)} = 1/40$ was 2 h 25 min.

4.2. Motion of an RBC subject to a quadrupolar fluid force

As a second numerical example we consider an RBC in a fluid occupying a square domain $\Omega = [-15\ \mu m, 15\ \mu m]^2$ with no-slip boundary conditions on all four boundary segments. We impose a *quadrupolar fluid force density* which is given as follows: For each velocity node i, $1 \leqslant i \leqslant n_1/2$, with coordinates $(x_i, y_i) \in \Omega$ we set $(\tilde{x}_i, \tilde{y}_i) := (x_i/D, y_i/D)$, $D = 15$ μm and define the components $u_{h,i}, u_{h,i+n_1/2}$ of a divergence-free velocity field $\mathbf{u}_h \in \mathbf{V}_h$ by

$$u_{h,i} := \pi v_0 \frac{\sin(\pi\tilde{x}_i)\ (2\cos(\pi\tilde{y}_i) - 1)}{(2 - \cos(\pi\tilde{x}_i))\ (2 - \cos(\pi\tilde{y}_i))^2}$$
$$u_{h,i+n_1/2} := -\pi v_0 \frac{\sin(\pi\tilde{y}_i)(2\cos(\pi\tilde{x}_i) - 1)}{(2 - \cos(\pi\tilde{x}_i))^2\ (2 - \cos(\pi\tilde{y}_i))}.$$

We introduce

$$f_{h,\text{quad}}^{(k+1)} := \mathbf{A}\mathbf{u}_h, \quad 0 \leqslant k \leqslant M - 1 \tag{4.1}$$

with the stiffness matrix $\mathbf{A}$ from Section 2.2 as an additional force density in (2.13). Moreover, we choose $T = 10$ as final time and $h = 1/16$, resulting in $n_1 + n_2 = 18050 + 2304 = 20\ 354$ degrees of freedom for the Navier–Stokes equations, and $\Delta q := h/2$ so that $N_3 = 128$. All other parameters are the same as in the first numerical example.

As can be seen in Fig. 4, the quadrupolar force density generates four pairwise counter-rotating vortices, and thus the induced flow is characterized by a velocity field that is rapidly varying in terms of magnitude and direction. The RBC, whose center $x = (-0.5\ \mu m, -1.0\ \mu m)^T$ is initially placed a little offside the origin, gets kneaded and spun around clockwise as time proceeds (see Fig. 5 (bottom)).

We note that in [19] a quadrupolar force field has been generated by surface acoustic waves, whereas in [23] a similarly defined quadrupolar force has been used for the separation of chiral objects in microflows.

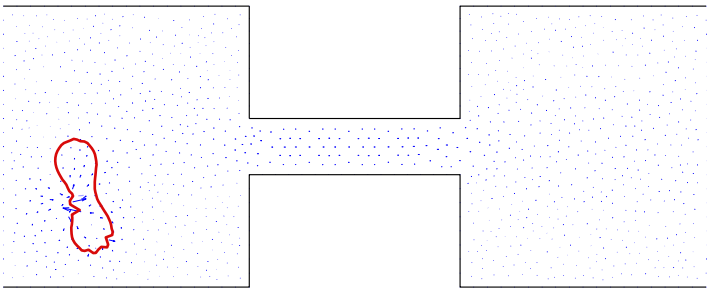

Fig. 1. Numerical instability of the BE/FE FE-IB for $\tau = 1/250$. The computation was stopped at $t = 0.05$ after one membrane node had left the domain (not shown in the figure) due to high oscillations.

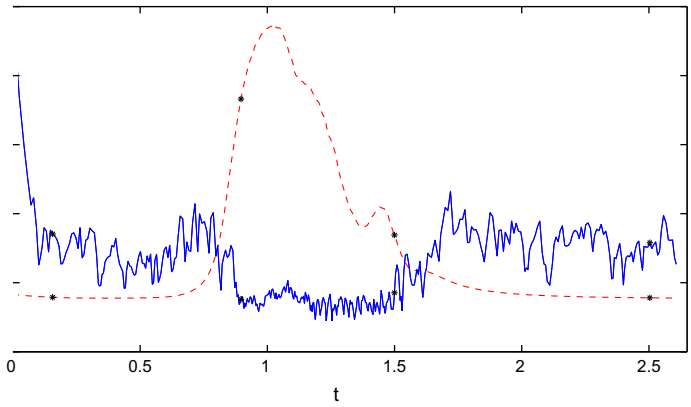

Fig. 2. Evolution of the adaptively chosen time increments (solid line) and of the (scaled) potential energy of the membrane (dashed line).

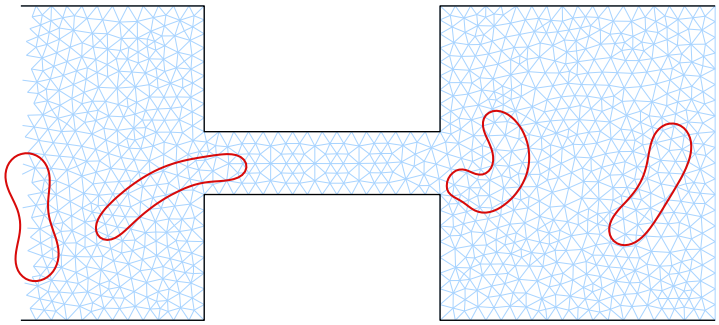

Fig. 3. Snapshots of the RBC's membrane at selected time instants. These time instants correspond to the $*$-marked instants in Fig. 2.

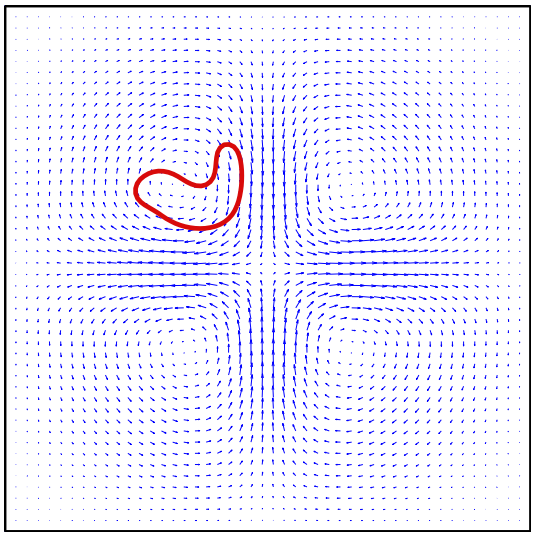

Fig. 4. A quadrupolar force density creates four pairwise counter-rotating vortices and significantly impacts the motion and deformation of an RBC.

We have run the example with two semi-implicit schemes (Backward Euler/Forward Euler (BE/FE), Crank-Nicolson/Forward Euler (CN/FE)) and the fully implicit scheme (BE/BE) featuring an adaptive time step selection. In Table 1, we provide a comparison of the three schemes in terms of computational time and average, minimal, and maximal time step size. The minimal time step of the fully implicit scheme is approximately 10 times larger than the constant time step sizes of the

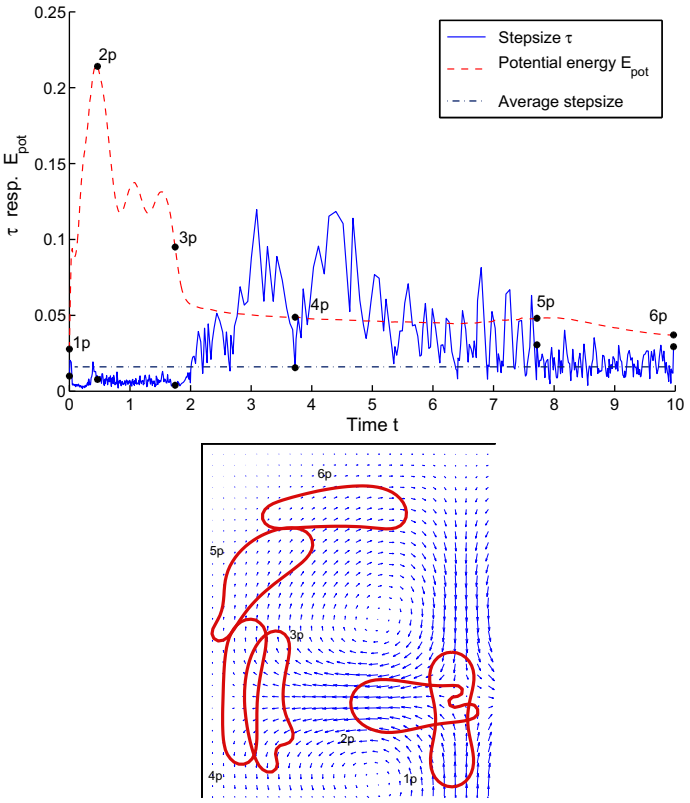

Fig. 5. The evolution of the adaptively chosen time steps and of the membrane's potential energy (top). The marked instants correspond to the snapshots in the picture below.

Table 1
Comparison of three different schemes for Example 2.

Scheme	Duration (min)	M	$\tau_{\varnothing}$	$\min_k(\tau_k)$	$\max_k(\tau_k)$
BE/FE	116.5	6500	1/650	1/650	1/650
CN/FE	112.0	6300	1/630	1/630	1/630
BE/BE	94.8	622	$1.60 \cdot 10^{-2}$	$1.76 \cdot 10^{-3}$	$1.20 \cdot 10^{-1}$

Table 2
Dependence of the fully implicit scheme w.r.t. the initial value $\tau_{(0.0)} := 1/\widehat{N}$.

$\widehat{N}$	Duration (min)	M	τ_{av}	$\min_k(\tau_k)$	$\max_k(\tau_k)$
10	(No convergence)				
20	(No convergence)				
30	(No convergence)				
40	94.5	616	$1.62 \cdot 10^{-2}$	$1.86 \cdot 10^{-3}$	$1.34 \cdot 10^{-1}$
60	93.1	609	$1.64 \cdot 10^{-2}$	$1.18 \cdot 10^{-3}$	$1.46 \cdot 10^{-1}$
80	94.7	620	$1.61 \cdot 10^{-2}$	$1.73 \cdot 10^{-3}$	$1.31 \cdot 10^{-1}$
100	94.8	622	$1.60 \cdot 10^{-2}$	$1.76 \cdot 10^{-3}$	$1.20 \cdot 10^{-1}$
150	98.3	621	$1.61 \cdot 10^{-2}$	$1.39 \cdot 10^{-3}$	$1.19 \cdot 10^{-1}$
200	98.5	627	$1.60 \cdot 10^{-2}$	$1.74 \cdot 10^{-3}$	$1.15 \cdot 10^{-1}$
250	96.9	614	$1.63 \cdot 10^{-2}$	$1.95 \cdot 10^{-3}$	$1.23 \cdot 10^{-1}$
300	97.9	617	$1.63 \cdot 10^{-2}$	$2.11 \cdot 10^{-3}$	$1.44 \cdot 10^{-1}$

semi-implicit schemes. The fully implicit scheme, for which again no τ-correction was necessary, is even faster than the semi-implicit ones. The reason is that for this example two critical situations occur (an initial squeezing of the RBC and a subsequent almost-collision with the left wall), where relatively small time step sizes must be chosen. This alternates with

'calm' situations where the adaptive scheme picks large time steps. In contrast, the semi-implicit schemes have to work with the same small time step throughout the whole computation.

On the other hand, a certain disadvantage of the fully implicit scheme is the need for significantly more memory, since the computation of certain sub-blocks of the Newton matrix containing second order derivatives by automatic differentiation (AD) is memory intensive.

The performance of the adaptive stepsize selection algorithm is relatively independent of the initial choice of the continuation parameter $\tau_{(0,0)}$. Table 2 displays the performance for different initial guesses and underlines the robustness of the algorithm with respect to changes in the initial data. If $\tau_{(0,0)}$ is chosen too large, the first Newton correction step at $t = 0 + \tau_{(0,0)}$ does not converge and the algorithm has to be stopped: this was the case for $\tau_{(0,0)} \geqslant 1/30$. We note that the time step sizes for both semi-implicit schemes given in Table 1 were found purely heuristically (increasing $\widetilde{N} := 1/\tau \in \mathbb{N}$ by 10-units as long as the scheme turns out to be stable). In general, the knowledge of a 'proper' step size is not available in advance.

5. Conclusion

The Immersed Boundary method (IB) is a powerful technique for the mathematical modeling and numerical simulation of fluid–structure interactions, but it is also known for its inherent stiffness. To cope with this problem, we have presented a fully implicit, fully variational version of the IB and a technique how to solve the resulting nonlinear systems of equations efficiently. It has been shown that the fully implicit scheme can be interpreted as a BE-approximation of a parameter-dependent nonlinear system of equations for which adaptive continuation strategies exist. More precisely, we have used a predictor–corrector strategy based on the affine-covariant Newton convergence theory developed in [15]. The idea is to use local information about the trajectory of state variables for the construction of the upcoming time increment. This is done in such a way that the convergence requirements of the Newton correction step, conducted at the next time instant, are likely to be met. We have shown that the associated Jacobians are invertible, if the time increment is chosen small enough, and thus the Newton iterations are well defined. The combination of an adaptively chosen time increment and a correction step leads to a numerically stable time-stepping scheme. This has been demonstrated by a challenging test problem where a red blood cell passes through a thin capillary and, in doing so, undergoes a rapid change in its potential energy which usually (i.e., in the semi-implicit case) leads to numerical instabilities.

Acknowledgments

The first author has been supported by NSF grants DMS-0707602, DMS-0810176, DMS-0811153, DMS-0914788, by the DFG within the Priority Programs SPP 1253 and SPP 1506, by the BMBF within the Collaborative Research Projects 'FROPT' and 'MeFreSim', and by the ESF within the Research Networking Programme 'OPTPDE'. The second author acknowledges support by the DFG within the Priority Program SPP 1253.

References

[1] M. Abkarian, C. Lartigue, A. Viallat, Tank treading and unbinding of deformable vesicles in shear flow: determination of the lift force, Phys. Rev. Lett. 88 (2002) 068103.
[2] M. Abkarian, A. Viallat, Dynamics of vesicles in a wall-bounded shear flow, Biophys. J. 89 (2005) 1055.
[3] B. Alberts, A. Johnson, J. Lewis, M. Raff, K. Roberts, P. Walter, Molekularbiologie der Zelle, Wiley-VCH, Weinheim, 2004.
[4] X. An, M.C. Lecomte, J.A. Chasis, N. Mohandas, W. Gratzer, Shear-response of the spectrin dimer–tetramer equilibrium in the red blood cell membrane, J. Biol. Chem. 277 (35) (2002) 31796–31800.
[5] P. Bagchi, P. Johnson, A. Popel, Computational fluid dynamic simulation of aggregation of deformable cells in a shear flow, J. Biomech. Eng. 127 (2005) 1070–1080.
[6] J. Beaucourt, F. Rioual, T. Seon, T. Biben, C. Misbah, Steady to unsteady dynamics of a vesicle in a flow, Phys. Rev. E 69 (2004) 011906.
[7] T. Biben, C. Misbah, Tumbling of vesicles under shear flow within an advected-field approach, Phys. Rev. E 67 (2003) 031908.
[8] D. Boffi, L. Gastaldi, A finite element approach for the immersed boundary method, Comput. Struct. 81 (2003) 491–501.
[9] D. Boffi, L. Gastaldi, L. Heltai, Numerical stability of the finite element immersed boundary method, Math. Model. Methods Appl. Sci. 17 (2007) 1479–1505.
[10] D. Boffi, L. Gastaldi, L. Heltai, On the CFL condition for the finite element immersed boundary method, Comput. Struct. 85 (2007) 775–783.
[11] D. Boffi, L. Gastaldi, L. Heltai, C. Peskin, On the hyper-elastic formulation of the immersed boundary method, Comput. Methods Appl. Mech. Eng. 197 (2008) 2210–2231.
[12] D. Braess, Finite Elements: Theory, Fast Solvers, and Applications in Solid Mechanics, third ed., Cambridge University Press, 2007.
[13] S.C. Brenner, R. Scott, The Mathematical Theory of Finite Element Methods, third ed., Springer, Berlin–Heidelberg–New York, 2008.
[14] F. Brezzi, M. Fortin, Mixed and Hybrid Finite Element Methods, Springer, Berlin–Heidelberg–New York, 1991.
[15] P. Deuflhard, Newton Mehtods for Nonlinear Problems – Affine Invariance and Adaptive Algorithms, Springer, Berlin–Heidelberg–New York, 2004.
[16] T. Franke, R.H.W. Hoppe, C. Linsenmann, L. Schmidt, C. Willbold, Numerical simulation of the motion of red blood cells and vesicles in microfluidic flows, Comput. Visualiz. Sci. 14 (2011) 167–180.
[17] C.D. Eggleton, A.S. Popel, Large deformation of red blood cell ghosts in simple shear flow, Phys. Fluids 10 (1998) 1834–1845.
[18] P. Grisvard, Elliptic Problems in Nonsmooth Domains, Pitman, Boston, 1985.
[19] Z. Guttenberg, A. Rathgeber, S. Keller, J.O. Radler, A. Wixforth, M. Kostur, M. Schindler, P. Talkner, Flow profiling of a surface-acoustic-wave nanopump, Phys. Rev. E 70 (2004) 056311.
[20] K. de Haas, C. Bloom, D. van den Ende, M. Duits, J. Mellema, Deformation of giant lipid bilayer vesicles in shear flow, Phys. Rev. E 56 (1997) 7132.
[21] V. Kantsler, V. Steinberg, Orientation and dynamics of a vesicle in tank-treading motion in shear flow, Phys. Rev. Lett. 95 (2005) 258101.
[22] S.R. Keller, R. Skalak, Motion of a tank-treading ellipsoidal particle in a shear flow, J. Fluid Mech. 120 (1982) 27.
[23] M. Kostur, M. Schindler, P. Talkner, P. Hänggi, Chiral separation in microflows, Phys. Rev. Lett. 96 (2006) 014502-1–014502-4.

[24] M. Kraus, W. Wintz, U. Seifert, R. Lipowsky, Fluid vesicles in shear flow, Phys. Rev. Lett. 77 (1996) 3685.
[25] D.V. Le, J. White, J. Peraire, K.M. Lim, B.C. Khoo, An implicit immersed boundary method for three-dimensional fluid-membrane interactions, J. Comput. Phys. 228 (2009) 8427–8445.
[26] P. Lee, B.E. Griffith, C.S. Peskin, The immersed boundary method for advection–electrodiffusion with implicit timestepping and local mesh refinement, J. Comput. Phys. 229 (2010) 5208–5227.
[27] Y. Mori, C.S. Peskin, Implicit second-order immersed boundary methods with boundary mass, Comput. Methods Appl. Mech. Eng. 197 (2008) 2049–2067.
[28] E.P. Newren, A.L. Fogelson, R.D. Guy, R.M. Kirby, Unconditionally stable discretizations of the immersed boundary equations, J. Comput. Phys. 222 (2007) 702–719.
[29] H. Noguchi, G. Gompper, L. Schmid, A. Wixforth, T. Franke, Dynamics of fluid vesicles in flow through structured microchannels, Eur. Phys. Lett., in press.
[30] T.-W. Pan, T. Wang, Dynamical simulation of red blood cell rheology in microvessels, Int. J. Numer. Anal. Model. 6 (2009) 455–473.
[31] C. Peskin, Numerical analysis of flood flow in the heart, J. Comput. Phys. 25 (1977) 220–252.
[32] C. Peskin, The immersed boundary method, Acta Numer. 11 (2002) 479–517.
[33] C. Peskin, D.M. McQueen, A three-dimensional computational method for blood flow in the heart. I. Immersed elastic fibers in a viscous incompressible fluid, J. Comput. Phys. 81 (1989) 372–405.
[34] C. Peskin, B. F Printz, Improved volume conservation in the computation of flows with immersed elastic boundaries, J. Comput. Phys. 105 (1993) 33–46.
[35] F. Rioual, T. Biben, C. Misbah, Analytical analysis of a vesicle tumbling under a shear flow, Phys. Rev. E 69 (2004) 061914.
[36] M.E. Rosar, C.S. Peskin, Fluid flow in collapsible elastic tubes: a three-dimensional numerical model, New York J. Math. 7 (2001) 281–302.
[37] S.M. Rump, INTLAB – INTerval LABoratory, in: T. Csendes (Ed.), Developments in Reliable Computing, Kluwer Academic Publishers, Dordrecht, 1999, pp. 77–104.
[38] U. Seifert, Fluid membranes in hydrodynamic flow fields: formalism, an application to fluctuating quasispherical vesicles in shear flow, Eur. Phys. J. B 8 (1999) 405.
[39] R. Skalak, S. Chien, Handbook of Bioengineering, McGraw-Hill, New York, 1987.
[40] L. Tartar, Introduction to Sobolev Spaces and Interpolation Theory, Springer, Berlin–Heidelberg–New York, 2007.
[41] V. Vitkova, M. Mader, T. Biben, T. Podgorski, Tumbling of lipid vesicles, enclosing a viscous fluid, under a shear flow, J. Optoelectron. Adv. Mater. 7 (2005) 261.
[42] T. Wang, T.-W. Pan, Z.W. Xing, R. Glowinski, Numerical simulation of red blood cell rouleaus in microchannels, Phys. Rev. E 79 (2009) 041916-1–041916-11.